

ILLINOIS TRANSIENT MODEL TWO-EQUATION MODEL V. 1.5

User's Manual

BY

Arturo León, Ph.D., P.E. (Computational Hydraulics)

Assistant Professor at Oregon State University (Corresponding author)

Email: arturo.leon@oregonstate.edu

Web page: <http://web.engr.oregonstate.edu/~leon/>

and

Nils Oberg (Graphical user interface)

Computer Science Engineer at University of Illinois at Urbana-Champaign

Oregon State University, Corvallis

March 2015

Acknowledgements



The ITM model would not have been possible without the financial support of the Metropolitan Water Reclamation District of Greater Chicago [<http://www.mwrd.org/irj/portal/anonymous/Home>] and of the Civil and Environmental Engineering Department of the University of Illinois at Urbana-Champaign (UIUC) [<http://www.cee.illinois.edu/>]). In particular, the first author wishes to express his sincere gratitude to Profs. Marcelo H. García (UIUC), Arthur R. Schmidt (UIUC) and Mohamed S. Ghidaoui (The Hong Kong University of Science and Technology) for their continuous support and guidance while the first author was a Ph.D. student and later a Post-doctoral Research Associate at the University of Illinois at Urbana-Champaign. Since 2008, the first author has received small contributions of consulting companies in the United States and around the world for technical assistance in running the ITM model. These contributions were used in full for continuing the further development of the ITM model. The current version of ITM was developed at Oregon State University (Corvallis) [<http://cce.oregonstate.edu/>, where the first author is a professor].

Abstract

The Illinois Transient Model (ITM) is a multi-purpose Finite Volume (FV) shock-capturing model for simulating transient flows in closed-conduit systems ranging from dry-bed flows, to gravity flows, to partly gravity-partly surcharged flows (mixed flows) to fully pressurized flows (waterhammer flows). The ITM model can handle complex boundary conditions such as dropshafts, reservoirs, closing and opening of gates (in open channel and pressurized flow regime), and junctions with any number of connecting pipes and any type of horizontal and vertical alignment. ITM can also simulate flows in adverse slopes.

The first versions of ITM were developed at the University of Illinois at Urbana-Champaign (Urbana). The current version of ITM was developed at Oregon State University (Corvallis), where the first author is a professor. ITM has features that make this model superior with respect to other models for analyzing transient flows in complex closed-conduit systems. The first feature is that the ITM model can simulate all possible flow regimes in complex closed-conduit systems. In particular, the ITM model can accurately describe positive and negative open channel-pressurized flow interfaces, interface reversals, and it can simulate sub-atmospheric pressures in the pressurized flow region. The second feature is that the ITM model can simulate transient mixed flows when large pressure wave celerities (~ 1000 m/s) are used. The latter is very important when pressurized transient flows are of interest. If transients are of no interest, a small pressure wave celerity may be used in the user's interface to speed up the computations.

The numerical code for the hydraulics of the ITM model was written from scratch by Dr. Arturo León [<http://web.engr.oregonstate.edu/~leon/>]. The graphical user interface of ITM was modified from the graphical user interface of the storm water management model (SWMM) originally developed by the US Environmental Protection Agency [<http://www.epa.gov/>].

Table of Contents

List of Figures	6
1 Introduction	1
1.1 What is the Illinois Transient Model (ITM) and what are the modeling capabilities	1
1.2 Common applications and limitations of the ITM model	2
1.3 Installing the ITM model	3
1.4 Steps in using the ITM model	3
1.5 About this manual	3
2 Model Updates.....	4
2.1 Improvement of ITM 1.5 with respect to ITM 1.3	4
3 Governing equations, numerical techniques and validation of the ITM model.....	5
3.1 Governing equations	6
3.2 Numerical solution of governing equations	9
3.3 Validation of the ITM model	10
3.3.1 Experiments type A of Trajkovic et al. (1999)	11
3.3.2 Experiments of Vasconcelos et al. (2006)	14
3.3.3 Hypothetical three-way merging flow	16
3.3.4 Hypothetical three-way dividing flow	21
3.3.5 Experiments of León et al. (2010b) - Oscillation tube ..	24
4 Working with the ITM model	28
4.1 Network representation	28
4.1.1 Conduits	28
4.1.2 Junctions	29
4.1.3 Reservoirs	29
4.1.4 Constant boundaries	30
4.1.5 Gate boundary	31
4.1.6 Rating curve boundary and Warning	32
4.2 ITM Simulation options	34
4.3 Volume mass conservation	35

5	ITM Examples	37
---	--------------------	----

List of Figures

3.1	Sketch of positive interface, negative interface and interface reversal.	8
3.2	Measured and computed pressure heads for type A experiments of Trajkovic et al. (1999).	13
3.3	Simulated pressure head snapshots for experiments of Vasconcelos et al. (2006)	15
3.4	Measured and computed velocities for experiments of Vasconcelos et al. (2006).	16
3.5	Measured and computed pressure heads for experiments of Vasconcelos et al. (2006)	17
3.6	Plan and profile view for three-way merging flow hypothetical case.	18
3.7	CFD mesh convergence for three-way merging flow test case.	19
3.8	Pressure head trace at mid-way of pipe 2 (three-way merging flow).	20
3.9	Pressure head trace at mid-way of pipe 3 (three-way merging flow).	20
3.10	Plan and section view for three-way dividing flow hypothetical case.	22
3.11	Pressure head trace at mid-way of pipe 1 (three-way dividing flow).	23
3.12	Pressure head trace at mid-way of pipe 2 (three-way dividing flow).	24
3.13	Experimental setup of León et al. (2010b).	26
3.14	CFD mesh convergence for oscillation tube test case (León et al. 2010b).	27
3.15	Water level elevation at upstream drop-shaft (León et al. 2010b).	27
4.1	Network elements supported by ITM.	29
4.2	Graphical editor for a conduit in ITM.	30
4.3	Graphical editor for a junction in ITM.	30
4.4	Graphical editor for a reservoir in ITM.	31
4.5	Graphical editor for a constant boundary.	32
4.6	Graphical editor for a gate boundary.	32
4.7	Graphical editor for a rating curve boundary.	33

4.8	Graphical editor for ITM simulation options.	34
4.9	System volume error (%).	35
4.10	System volume error (m^3).	36
5.1	Layout of the hypothetical system showing the nodes.	39
5.2	Layout of the hypothetical system showing the conduits or links.	40
5.3	One of the inflow hydrographs used for this example.	41
5.4	Outflow discharge versus water depth for the rating curve boundary.	42
5.5	Time series of gate opening in percentage.	43
5.6	Curve of gate head loss coefficient versus gate opening in percentage ($k = 1/C_d^2$, where C_d = discharge coefficient)	44
5.7	Dates in the “Simulation options” for the coarse output time.	45
5.8	Time steps in the “Simulation options” for the coarse output time.	46
5.9	Dates in the “Simulation options” for the fine output time.	47
5.10	Time steps in the “Simulation options” for the fine output time.	48
5.11	Interface for setting up the HOTSTART option in ITM.	49
5.12	Interface for saving HOTSTART file.	50
5.13	Interface for using HOTSTART file in new simulation.	51
5.14	ITM parameters in the “Simulation options”.	52
5.15	Piezometric depth traces at the center of various tunnel reaches for the coarse output time (Initial dry bed state, $a = 200 m/s$).	53
5.16	Flow velocity traces at the center of various tunnel reaches for the coarse output time (Initial dry bed state, $a = 200 m/s$).	54
5.17	Flow discharge traces at the center of various tunnel reaches for the coarse output time (Initial dry bed state, $a = 200 m/s$).	55
5.18	Zoom-in of region “A” in Fig. 5.15 using fine output time	56
5.19	Depth versus flow discharge (“rating curve”) for the link 2026 (mid-way of tunnel) (Initial dry bed state, $a = 200 m/s$).	57
5.20	Typical user-defined table.	58
5.21	Typical text report.	59
5.22	Hydraulic grade line snapshot between nodes DS15 and RatingCurve1 after 00 h 00 min 02 sec (Initial dry bed state, $a = 200 m/s$).	60
5.23	Hydraulic grade line snapshot between nodes DS15 and RatingCurve1 after 09 h 00 min 00 sec (Initial dry bed state, $a = 200 m/s$).	61
5.24	Hydraulic grade line snapshot between nodes DS15 and RatingCurve1 after 13 h 26 min 50 sec (Initial dry bed state, $a = 200 m/s$).	62
5.25	Hydraulic grade line snapshot between an upstream node and RatingCurve1 after 20 h 40 min 58 sec (Initial dry bed state, $a = 200 m/s$).	63

5.26	Debug file intended for debugging of errors.	64
5.27	ITM interface for plotting time traces of volume errors.	65
5.28	System volume error (%)[fine output time].	66
5.29	System volume error (m ³)[fine output time].	66

Chapter 1

Introduction

1.1 What is the Illinois Transient Model (ITM) and what are the modeling capabilities

The Illinois Transient Model (ITM) is a multipurpose Finite Volume (FV) shock-capturing model to analyze transient flows in closed-conduit systems ranging from dry-bed flows to gravity flows, to partly gravity-partly surcharged flows (mixed flows) to fully pressurized flows (waterhammer flows). The ITM model can handle complex boundary conditions such as dropshafts, reservoirs, closing and opening of gates (in open channel and pressurized flow regime), and junctions with any number of connecting pipes and any type of horizontal and vertical alignment. ITM can also simulate flows in adverse slopes.

For a comprehensive description of the governing equations and the numerical methods used in the ITM model the reader is referred to León (2006), León et al. (2006, 2008, 2010a, 2010b, 2013).

Historically, the ITM model was first developed in 2004 using a modified Preissmann slot approach (one-governing equation) for simulating mixed flows. The 2004 version of the ITM model, as other Preissmann-slot based models has the inability of simulating negative pressures. Because negative pressures are very common in pressurized transient flows, it was decided to change the approach for handling mixed flows. The second version of the ITM model was completed in 2006. In the 2006 version of the ITM model, the free surface region is modeled using the 1D Saint-Venant equations, the pressurized region is modeled using the 1D compressible waterhammer equations and open channel-pressurized flow interfaces are modeled by enforcing mass, momentum and energy relations across the interfaces together with Riemann solvers at the sides of the mixed flow interfaces. This version of the ITM model is referred as the two-equation model. The current version of the ITM model is an improved version of the 2006 ITM model based on León et al. (2010a, 2010b, 2013).

The current version of the ITM model has features that make this model superior with respect to other models for analyzing transient flows in complex closed-conduit systems. The first feature is that the ITM model can

simulate all possible flow regimes in complex closed-conduit systems. In particular, the ITM model can accurately describe positive and negative open channel-pressurized flow interfaces, interface reversals, and it can simulate sub-atmospheric pressures in the pressurized flow region. Song et al. (1983) defined an open channel-pressurized (mixed) flow interface as positive if it is moving towards the open-channel flow, and negative or retreating if it is moving towards the region of pressurized flow. The change in direction of the interface from positive to negative is called interface reversal. The second feature is that the ITM model can simulate transient mixed flows when large pressure wave celerities (~ 1000 m/s) are used. The latter is very important when pressurized transient flows are of interest. If transients are of no interest, a small pressure wave celerity may be used to speed up the computations.

The graphical user interface of the ITM model was modified from the graphical user interface of the Storm Water Management Model (SWMM) originally developed by the U.S. EPA.

1.2 Common applications and limitations of the ITM model

ITM was used for the analysis of combined sewer systems in the United States of cities like Chicago, Omaha, Cleveland, St. Louis and Dallas and internationally in countries such as Switzerland, New Zealand, France and Mexico. ITM has been used in particular to: (1) assess the impact of gate closures in the generation of transients in combined sewer systems; (2) study transient phenomena and conveyance capacity in combined sewer systems associated to heavy rainfall events. The ITM model can be used in transient and non-transient conditions. If transients are of no interest, a small pressure wave celerity may be used to speed up the computations.

Overall, the ITM model can be used for simulating all possible flow regimes in complex closed-conduit systems ranging from dry-bed flows to gravity flows, to partly gravity-partly surcharged flows (mixed flows) to fully pressurized flows. The boundary conditions currently supported include drop-shafts, reservoirs, constant flow or pressure, closing and opening of gates in pressurized flow conditions as a function of time, and junctions with any number of connecting pipes and any type of horizontal and vertical alignment.

The ITM model has the intrinsic limitations of a one-dimensional model. However, it has been shown in various publications that the ITM model can predict with good accuracy pressure and flow discharge fluctuations under free surface, pressurized and mixed flow conditions.

1.3 Installing the ITM model

The ITM model was designed to run under Windows. It is distributed as a collection of files in a compressed archive. To install ITM the archive needs to be uncompressed. Choose a folder on your hard drive, such as C:\ITM, and put all of the files in there. Once the files have been extracted from the archive, then ITM can be run by double-clicking on the ITM.exe program. It is important that all of the files, many of which are DLL files, remain in the same directory as the ITM.exe program. Failing to follow these directions may prevent ITM from running.

1.4 Steps in using the ITM model

The steps for using the ITM model are (for details see Chapters 4 and 5):

1. Draw a network representation of the physical components of the closed-conduit system.
2. Add inflow hydrographs.
3. Edit the properties of the objects that make up the system.
4. Specify the set of options for the simulation.
5. Run the simulation.
6. View the results of the simulation.

1.5 About this manual

Chapter 1: Introduction.

Chapter 2: Model Updates This chapter presents a brief summary of the updates of the ITM model.

Chapter 3: Governing equations, numerical techniques and validation of the ITM model. This chapter presents a brief description of the governing equations and the numerical techniques used for implementing the ITM model. This chapter also presents a description of various test cases used for the validation of the ITM model.

Chapter 4: Working with the ITM model. This chapter presents a brief description of new attributes unique to the ITM model to help get started using ITM.

Chapter 5: ITM Examples. This chapter presents examples for setting input data, running the model and visualizing results.

Chapter 2

Model Updates

2.1 Improvement of ITM 1.5 with respect to ITM 1.3

The major improvements are summarized below:

1. The tolerances (e.g., normal, high, etc) are removed from the graphical user interface (GUI) of ITM. The tolerances are now hard coded internally in ITM. This was made to allow the usage of ITM by less technical users;
2. The equations used in most boundary conditions (e.g., junction and drop-shaft) were normalized for faster convergence and less problems of non-convergence. In other words, the residuals of the non-linear systems of equations for each BC are now in the same units;
3. The version 1.5 includes three examples of near-actual combined sewer systems. The examples were modified from the actual configuration due to security and liability issues.

Chapter 3

Governing equations, numerical techniques and validation of the ITM model

The ITM model was built upon our earlier work and the work of others for simulating free surface flows, pressurized flows and mixed flows (simultaneous occurrence of free surface and pressurized flows). For a comprehensive description of the governing equations and the numerical methods used in the ITM model the reader is referred to León (2006), León et al. (2006, 2008, 2010a, 2010b, 2013). In the ITM model the free surface region is simulated using the 1D Saint-Venant equations, the pressurized region is simulated using the classical 1D compressible waterhammer equations and open channel-pressurized flow interfaces are simulated by enforcing mass, momentum and energy relations across open channel-pressurized flow interfaces.

The ITM model can accurately describe complex flow features, such as positive and negative mixed flow interfaces, interface reversals and open channel bores. In particular, the ITM model can simulate negative interfaces in mixed flow conditions having supercritical flow in the free surface region. The authors are not aware of any existing mixed flow model that was formulated for negative interfaces when the flow in the free surface region is supercritical. The ITM model can also simulate negative pressures in pressurized flow regime.

Furthermore, the ITM model can simulate mixed flow conditions for a large range of pressure wave celerities (~ 1000 m/s) compared to current models. Current mixed flow models use small values of the pressure wave celerity in order to avoid numerical instabilities (e.g., Trajkovic et al. 1999, Vasconcelos et al. 2006). As is shown in León et al. 2010b, when there is interaction of pressurized waves, the results for the maximum pressure heads are highly dependent on the selection of the pressure wave celerity.

3.1 Governing equations

The one-dimensional open-channel and compressible water hammer flow continuity and momentum equations for prismatic conduits are written in their vector conservative form as follows (e.g. Guinot 2003, León 2006, León et al. 2006, 2008):

$$\frac{\partial \mathbf{U}}{\partial t} + \frac{\partial \mathbf{F}}{\partial x} = \mathbf{S} \quad (3.1)$$

where the vector variable \mathbf{U} , the flux vector \mathbf{F} and the source term vector \mathbf{S} for open-channel flows may be written as (e.g., León 2006, León et al. 2006):

$$\mathbf{U} = \begin{bmatrix} \rho A \\ \rho Q \end{bmatrix}, \mathbf{F} = \begin{bmatrix} \rho Q \\ \rho \frac{Q^2}{A} + A\bar{p} \end{bmatrix} \text{ and } \mathbf{S} = \begin{bmatrix} 0 \\ (S_o - S_e)\rho g A \end{bmatrix} \quad (3.2)$$

and for compressible water hammer flows as (e.g., Guinot 2003, León 2006, León et al. 2008):

$$\mathbf{U} = \begin{bmatrix} \rho_f A_f \\ \rho_f Q \end{bmatrix}, \mathbf{F} = \begin{bmatrix} \rho_f Q \\ \rho_f \frac{Q^2}{A_f} + A_f p \end{bmatrix} \text{ and } \mathbf{S} = \begin{bmatrix} 0 \\ (S_o - S_e)\rho_f g A_f \end{bmatrix} \quad (3.3)$$

where the variables for free surface flows are: A = cross-sectional area of the flow; Q = flow discharge; \bar{p} = average pressure of the water column over the cross sectional area; ρ = liquid density (assumed constant for free surface flows but not for pressurized flows); g = gravitational acceleration; S_o = bottom slope of the conduit; and S_e = slope of the energy line. The variables for compressible water hammer flows (pressurized flows) are: A_f = full cross-sectional area of the conduit, p = pressure acting on the center of gravity of A_f , and ρ_f = fluid density for compressible water hammer flows.

Eq. (3.1) for compressible waterhammer flows does not form a closed system in that the flow is described using three variables: ρ_f , p and Q . However, it is possible to eliminate the pressure variable by using the general definition of the pressure wave celerity (a_g), which relates p and ρ_f (e.g., Guinot 2003)

$$a_g = \left[\frac{d(A_f p)}{d(A_f \rho_f)} \right]^{1/2} \quad (3.4)$$

The wave celerity in single-phase (pure liquid) pressurized flows (a) is assumed to be constant (e.g., Wylie and Streeter 1983) and can be estimated using the following relation that is derived from classical structural mechanics (e.g., Wylie and Streeter 1983):

$$a = \left[\frac{k_f / \rho_{ref}}{1 + \frac{k_f d}{E e}} \right]^{1/2} \quad (3.5)$$

where ρ_{ref} is a reference density, d is the pipe diameter, e is wall thickness, E is Young's modulus of elasticity of the pipe material and k_f is the compressibility of the fluid in the pipe. Assuming an infinitely rigid pipe (e.g., A_f is assumed to be constant) and substituting a_g by a in Eq. (3.4), the integration of the differentials $d\rho_f$ and dp in Eq. (3.4) gives the following equation that relates p and ρ_f (León et al. 2007, 2008)

$$p = p_{ref} + a^2(\rho_f - \rho_{ref}) \quad (3.6)$$

where p_{ref} is a reference pressure. In free surface flows, the gravity wavespeed c is given by $c = \sqrt{gA/T}$ where T is the topwidth of the flow. According to this relation, the gravity wavespeed is unbounded as the water depth approaches the crown of the conduit. When the water depth approaches the crown of the conduit, the pressure wave and not the gravity wave should become the primary mode of propagation of a disturbance. In fact, experiments in circular pipes (e.g., Hamam and McCorquodale 1982) showed that flow instabilities occur for water depths greater than $0.8d$, causing oscillations that will lead to a sudden jump to pressurized flow. In the ITM model, the phase change from free surface to pressurized flow (not from pressurized to free surface flow) is assumed to occur when the water depth exceeds $y = y_{ref}$, where y is the water depth and y_{ref} is a reference depth. At this threshold condition ($y = y_{ref}$), all the flow parameters (e.g., fluid density, hydraulic area and average pressure) in both open-channel and pressurized flow regime have to be the same. Herein, y_{ref} is set equal to $0.95d$. It is pointed out that the results are not sensitive to y_{ref} . However, when using a small value of y_{ref} , large mass conservation errors may be attained. The reference area (A_{ref}) is the hydraulic area below $y_{ref} = 0.95d$ and A_f in the previous equations is replaced with A_{ref} . This results in a reduction of the hydraulic area for pressurized flows of less than 2%. When using the present model to simulate pure pressurized flows, A_{ref} can be set equal to A_f . In this way, the reduction in hydraulic area for pressurized flows (less than 2%) assumed when simulating mixed flows is eliminated. The assumed reference density (ρ_{ref}) is 1000 kg/m^3 that corresponds to clean water at a temperature of 4 degrees Celsius. For the phase change from pressurized to free surface flow (depressurization) the criteria given in Yuan (1984) is used.

Although the free surface and pressurized flow governing equations are mathematically similar (i.e., both hyperbolic), the physics of these flows have marked differences. One important distinction between these flows is the ability of pressurized flows to sustain sub-atmospheric pressures. Another important difference is that in pressurized flows a disturbance is propagated at a speed that is two orders of magnitude faster than in free surface flows. A moving interfacial boundary separates the two flow regimes. Song et al. (1983), Cardle (1984) among other authors defined an open channel-pressurized (mixed) flow interface as positive if it is moving towards the open-channel flow (Fig. 3.1

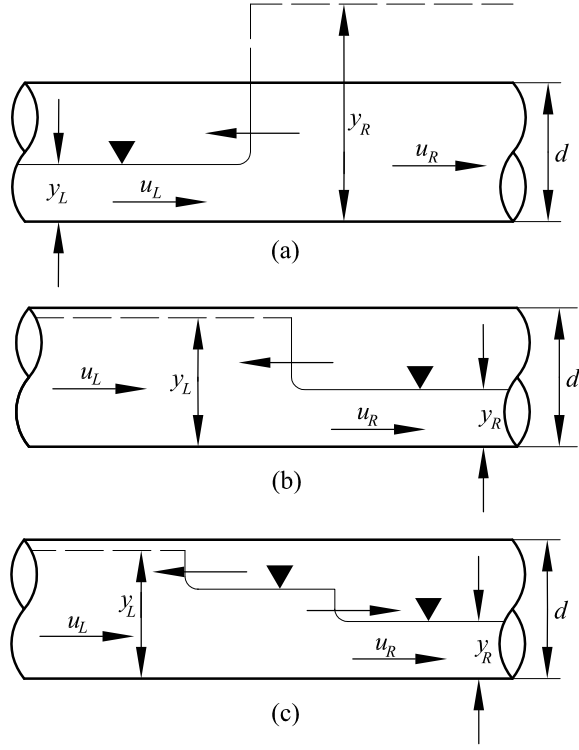


Figure 3.1: (a) Positive interface moving in the upstream direction (e.g., generated by sudden closure of a downstream gate) (b) Negative interface moving in the upstream direction (e.g., generated by depressurization at the downstream end of the system (c) Interface reversal.

(a)), and negative or retreating if it is moving towards the region of pressurized flow (Fig. 3.1 (b)). The change in direction of the interface from positive to negative is called interface reversal (Fig. 3.1 (c)). The direction and speed magnitude of a mixed flow interface can be determined using the following relation (e.g., Song et al. 1983)

$$w(t^n) = \frac{Q_R - Q_L}{A_R - A_L} \quad (3.7)$$

where a positive sign indicates that the interface is moving downstream and upstream otherwise.

The flow variables used in this manual are (ρA) and (ρQ) for free surface flows, and $(\rho_f A_f)$ and $(\rho_f Q_f)$ for pressurized flows. However, the engineering community prefers to use the piezometric head h and flow discharge Q . The latter variables can be determined from the flow variables used as follows:

- Free surface flow,

$$\begin{aligned} h &= y && (\text{where } y \text{ is a geometric function of } A) \\ Q &= (\rho Q)/\rho_{ref} && (\rho = \rho_{ref} \text{ for free surface flow}) \end{aligned} \quad (3.8)$$

- Pressurized flow,

$$\begin{aligned} h &= y_{ref} + \frac{a^2}{g} \left(\frac{\rho_f A_f}{\rho_{ref} A_{ref}} - 1 \right) \\ Q &= \frac{(\rho_f Q_f)}{(\rho_f A_f)} A_f \end{aligned} \quad (3.9)$$

where h is measured over the conduit bottom.

Following the criteria for determining if the flow is in free surface or pressurized flow regime is given. After a given node has been pressurized, free surface flow is not necessarily generated at this node when its head drops below the pipe crown. As reported by several researchers (e.g., Cardle 1984, Yuan 1984, Cardle et al. 1989), in negative interfaces there is a negative pressure on the pressurized side of the interface. In the latter case, the conditions given in Yuan (1984) for negative interfaces are used for the depressurization of the node. Furthermore, when a pipe system has been fully pressurized, the only way to start the depressurization process is through ventilated boundaries (e.g., dropshafts, reservoirs, etc).

3.2 Numerical solution of governing equations

The numerical scheme used in the ITM model is an explicit Finite Volume (FV) Godunov-type method. FV methods have the ability to capture discontinuities (e.g., shocks) in the solution automatically, without explicitly tracking them (e.g., Toro 2001). The FV method is based on writing the governing equations in integral form over an elementary control volume or cell, hence the general term of Finite Volume (FV) method. The computational grid or cell involves discretization of the spatial domain x into cells of length Δx_i and the temporal domain t into intervals of duration Δt . The i th cell is centered at node i and extends from $i - 1/2$ to $i + 1/2$. The flow variables (A and Q) are defined at the cell centers i and represent their average value within each cell. Fluxes, on the other hand are evaluated at the interfaces between cells ($i - 1/2$ and $i + 1/2$). For the i th cell, the updating FV formula for the left side of Eq. (3.1) is given by (e.g., Toro 2001, LeVeque 2002):

$$\mathbf{U}_i^{n+1} = \mathbf{U}_i^n - \frac{\Delta t}{\Delta x_i} (\mathbf{F}_{i+1/2}^n - \mathbf{F}_{i-1/2}^n) \quad (3.10)$$

where the superscripts n and $n + 1$ reflect the t and $t + \Delta t$ time levels, respectively. In Eq. (3.10), the determination of \mathbf{U} at the new time step $n + 1$

requires computation of the numerical flux (\mathbf{F}) at the cell interfaces at the old time n . To introduce the source terms (right side of Eq. 3.1) into the solution, a first-order time splitting method is used which takes into account an algorithm for ensuring that stationary flows don't produce unphysical flows. In the Godunov approach (Godunov 1959), the flux $\mathbf{F}_{i+1/2}^n$ is obtained by solving the Riemann problem with constant states \mathbf{U}_i^n and \mathbf{U}_i^{n+1} . This way of computing the flux leads to first-order accuracy of the numerical solution. To achieve second-order accuracy in space and time in the ITM model, the MUSCL - Hancock method (e.g., Toro 2001) was used. Second or higher order schemes are prone to spurious oscillations in the vicinity of discontinuities. To preserve the second-order accuracy of the solution away from discontinuities, while ensuring that the solution is oscillation-free near shock waves and other sharp flow features, a Total Variation Diminishing (TVD) method was used in the ITM model. The TVD property of the MUSCL - Hancock method is ensured by applying the MINMOD pre-processing slope limiter (see Toro 2001). For a comprehensive description of the numerical method used in the ITM model for free surface, pressurized and mixed flows, the reader is referred to León (2006), León et al. (2006, 2008, 2010a, 2013).

With regard to the boundary conditions (BCs) used in the ITM model the reader is referred to León et al. (2010b). León et al. (2010b) presented a general boundary condition for transient flows in a drop-shaft connected to an arbitrary number of pipes. This BC is general in the sense that it handles all possible flow regimes and their combinations at a junction.

3.3 Validation of the ITM model

The purpose of this section is to evaluate the accuracy and robustness of the ITM model for simulating transient free surface flows, pressurized flows and mixed flows in storm-sewers. Because of the lack of experimental data for complex test cases (e.g., complex boundaries), some of the test cases presented herein consider hypothetical storm-sewer systems (e.g., a three-way merging flow system and a three-way dividing flow system). A three-way merging flow consists of two inflowing pipes and one outflowing pipe and a three-way dividing flow boundary consists of one inflowing pipe and two outflowing pipes. For evaluating the hypothetical tests, Computational Fluid Dynamics (CFD) modeling results were used as frame of comparison. Two state-of-the-art CFD codes were used, namely FLOW-3D (Flow Science, Inc. 2005). and OpenFOAM (OpenCFD, Ltd. 2007). Unlike OpenFOAM, FLOW-3D has a module that allows modeling acoustic waves in pressurized flow conditions. The propagation of acoustic waves is associated with the compressibility of the flow; however not all CFD compressible models can simulate acoustic waves. It is acknowledged that the ITM model has been validated with more test cases than those presented in this section. The reader is referred to León (2006),

León et al. (2006, 2008, 2009, 2010a, 2010b, 2013) for a description of all test cases used for validating the ITM model. Five test cases are considered in this section. These are:

1. Experiments type A of Trajkovic et al. (1999) [Mixed flow].
2. Experiment of Vasconcelos et al. (2006). [Fully-pressurized flow].
3. Hypothetical three-way merging flow [Mixed flow].
4. Hypothetical Three-way dividing flow [Mixed flow].
5. Experiments of León et al. (2010b) [Fully-pressurized flow].

3.3.1 Experiments type A of Trajkovic et al. (1999)

In this test case, the ITM model is used to reproduce a set of experiments conducted at the Hydraulics Laboratory of University of Calabria by Trajkovic et al. (1999). In this test case, the ability of the ITM model to simulate a positive mixed flow interface reversing its direction and becoming a negative interface is tested. The experimental setup consisted of a perspex pipe ($n_m = 0.008 \text{ m}^{1/6}$) about 10 m long, having an inner diameter of 10 cm. Upstream and downstream tanks were connected to the pipe with automatic sluice gates. The experimental investigations evaluated the effect of rapid changes in the opening or closing of the sluice gates. Acknowledging the possible interference of the air phase in case the pipe became pressurized, several vents were placed at the top of the pipe.

In this test case, the type A set of experiments in Trajkovic et al. (1999) is considered. The initial conditions for this set of experiments were inflow rate constant at $0.0013 \text{ m}^3/\text{s}$, the bed slope at 2.7% (supercritical flow with an initial Froude number equal to 2.9), the upstream sluice gate opened $e_1 = 0.014 \text{ m}$, and the downstream sluice gate totally opened. The transient flow was generated after a rapid (but not instantaneous) closure of the downstream sluice gate that caused the formation of an open channel surge moving upstream. This surge was continuously strengthen by the inflow and after few seconds became a positive mixed flow interface that moved upstream. After 30 seconds of the gate closure, the gate was partially reopened. When the area of reopening was small, the positive interface continued to move upstream without retreating back downstream. When the area of reopening was about 10% or higher than the cross-sectional area of the pipe, the positive interface continued to move upstream propelled by its own inertia but after a short time the positive interface reversed its direction becoming a negative interface. Different values for the reopening (e_2) were tested. In this test case, three values for the reopening are considered: $e_2 = 0.008 \text{ m}$, $e_2 = 0.015 \text{ m}$, and $e_2 = 0.028 \text{ m}$.

Simulated (ITM and Trajkovic et al. (1999) model) and measured pressure traces at 0.6 m from the downstream gate for the three reopenings are shown in Fig. 3.2. The results shown in this figure for the ITM model were generated using 400 cells, a Courant number (Cr) of 0.80 and a pressure wave celerity of 500 m/s (estimated using Eq. 3.5). The results presented in Fig. 3.2 labeled Trajkovic et al. were obtained from Trajkovic et al. (1999). The results of the model of Trajkovic et al. (1999) were generated using a pressure wave celerity of about 4 m/s. Even though the comparison of results between our model and that of Trajkovic et al. (1999) may not seem relevant because different pressure wave celerities were used, the results may help to point out that our model is robust for large pressure wave celerities.

As can be observed in Fig. 3.2, the simulated pressure head (h) traces for both numerical models have a good agreement with the corresponding experimental measurements. In particular, the formation of the filling bore and its velocity of propagation are accurately predicted by both models. However, all the computed shock fronts are steeper than the measured ones. This is because in the experiments the closing of the gate was rapid, but not instantaneous, as was assumed in the simulations.

Fig. 3.2 also shows a drop in the pressure head after the partial reopening of the downstream gate ($t = 30$ s). In the simulations (both models), an instantaneous partial reopening was assumed which caused a steeper front of the pressure drop compared to the experimental results. The smaller pressure drop in the simulations (both models) may be in part due to the inaccuracies in representing the partial opening at the downstream boundary. At this boundary, the orifice equation of Trajkovic et al. (1999) was used.

For a reopening of 0.008 m [Fig. 3.2(a)], after a small drop in the pressure head, the pressure head continuously increased in all sections (both models and experiment). This is because the outflow from the pipe was smaller than the inflow. For a reopening of 0.015 m [Fig. 3.2(b)], a stationary mixed flow interface was observed and computed (experiment and ITM model only) in the pipe after the drop in the pressure head. For a reopening of 0.028 m [Fig. 3.2(c)], the mixed flow interface traveled downstream (experiment and ITM model only), because the outflow was greater than the inflow. It is acknowledged that in Trajkovic et al. (1999) the numerical results for a reopening of 0.015 and 0.028 m [Figs. 3.2(b) and 3.2(c)] are not shown after about $t = 32$ s (shortly after gate is partially reopened). These authors reported numerical instabilities, even when a small wave celerity was used (~ 4 m/s).

As is pointed out by several authors (e.g., Trajkovic et al. 1999, Vasconcelos et al. 2006, León et al. 2009), the results are almost independent of the pressure wave celerity when simulating mixed flows in a single pipe, in which the pressurized flow region is isolated and when there is no interaction of pressurized waves. This explains why researchers using very low pressure wave celerities obtained good agreement with experiments when simulating mixed

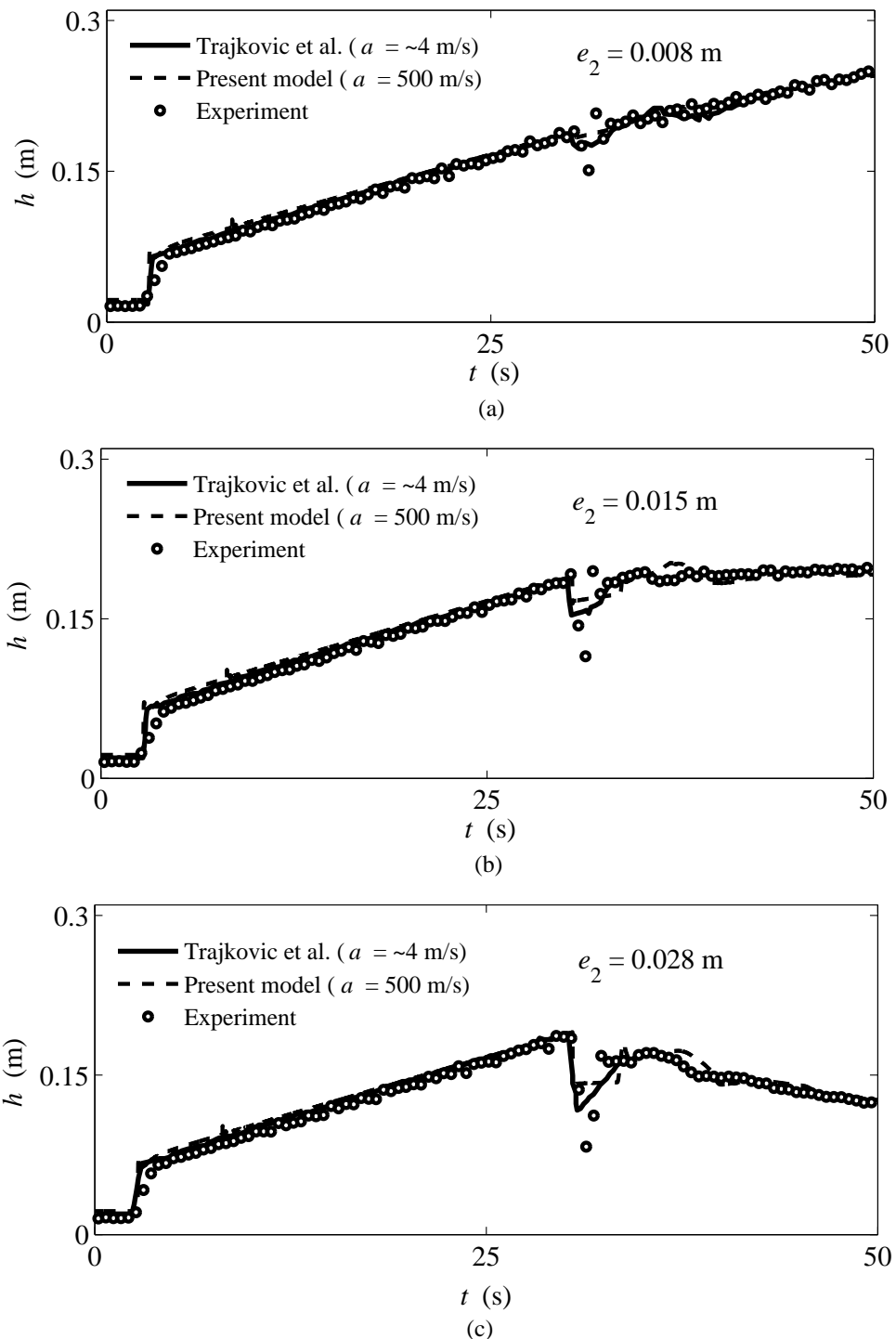


Figure 3.2: Measured and computed pressure heads at 0.6 m from downstream gate for type A experiments of Trajkovic et al. (1999).

flows. However, as is shown in León et al. 2010b, when there is interaction of pressurized waves such as in the case of multiple pipes; the results are highly dependent on the selection of the pressure wave celerity. In the latter case only a pressure wave celerity equal to the water hammer wavespeed gives accurate results on the propagation speed and magnitude of pressurized transients.

From Figs. 3.2(b) and 3.2(c), the reader can notice that shortly after the gate was reopened 0.015 m or 0.028 m, the positive interface reversed its direction becoming a negative interface. This is particularly clear for a reopening of 0.028 m [Fig. 3.2(c)]. Also, the initial Froude number of the flow was about 2.9 that corresponds to supercritical flow. As we mentioned earlier, the ITM model can simulate mixed flows without restriction of the type of flow in the free surface region. Figs. 3.2(b) and 3.2(c) show that our model can simulate a negative interface when the flow in the free surface region is supercritical.

3.3.2 Experiments of Vasconcelos et al. (2006)

The purpose of this section is to test the ability of the ITM model in simulating sub-atmospheric pressures in pressurized flow regime. The experiment used in this section was conducted at the University of Michigan and is reported in Vasconcelos et al. (2006). The experimental setup consisted of an acrylic pipeline 14.33 m long, having an inner diameter of 9.4 cm. The center portion of this pipe was raised about 15 cm with respect to both ends in order to create conditions for the occurrence of sub-atmospheric pressures. The pipeline was connected at its upstream end by a box tank and by a cylindrical tank at its downstream end. The experiment considered was obtained by filling the system to a level of 0.30 m at the box tank and the system allowed to come to rest. Then a siphon outflow was suddenly initiated at the box tank ($t = 0$). After some time, the water level in the box tank decreased to a level that created sub-atmospheric pressures at the center portion of the pipe. When the water level at the box tank dropped below the pipe crown just downstream of this tank, a complex flow pattern was developed. In this case, the flow just downstream of the box tank was in sub-atmospheric conditions, and under these conditions, air flow flowed from the tank into the pipe. This constitutes a two-phase flow problem that is outside of the scope of this work. The intrusion of air flow in the experiment occurred at about $t = 42.5$ s, and in the model about 1.7 seconds earlier. Since our work is limited to single-phase flows, the comparison between model prediction and experimental results are presented until right before the occurrence of air intrusion only ($t < \approx 40.8$ s).

To show the sequence of the formation of sub-atmospheric pressures, simulated pressure head snapshots at different times are presented in Fig. 3.3. When using the present model to simulate fully pressurized flows, as in this test case, A_{ref} can be set equal to A_f (full cross-sectional area of the conduit). In this way, the about 2% reduction in hydraulic area for pressurized flows as-

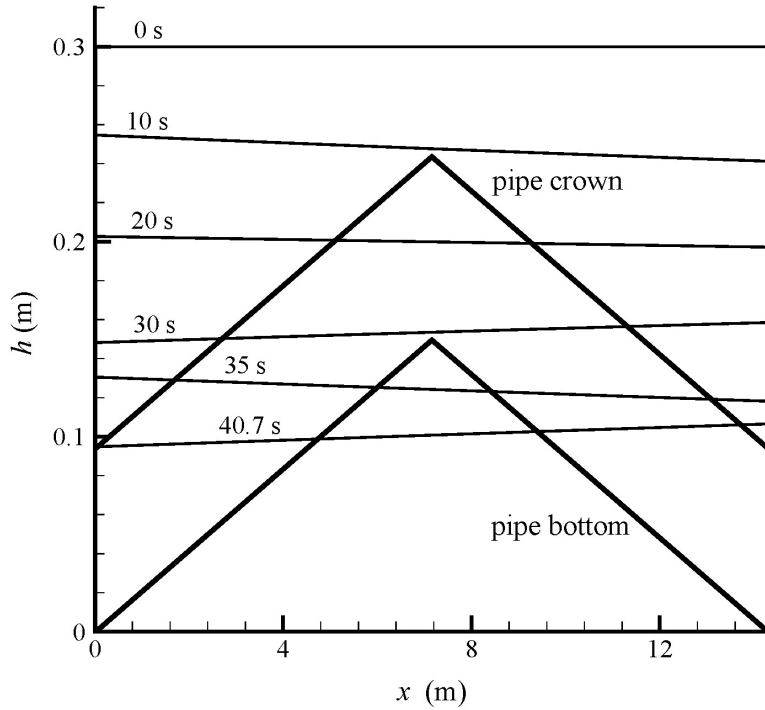


Figure 3.3: Simulated pressure head snapshots for experiments of Vasconcelos et al. (2006).

sumed when simulating mixed flows is eliminated. The pressure wave celerity used in the simulations was 300 m/s based on experimental measurements of pressure pulse propagation. The outflow was assumed constant and a value of 0.45 L/s was estimated by observing the change in water volume over time. For estimating energy losses, Vasconcelos et al. (2006) used a Manning roughness of $0.012 \text{ m}^{1/6}$. However the Manning's equation is applicable to fully rough flows only. Since the experiments were performed in laminar and transitional flow conditions ($Re < 4300$), the Darcy-Weisbach equation, which is applicable to laminar, transitional and fully rough flows would be a better estimate for the energy losses. For comparison, the numerical simulations were performed using the equations of Manning and Darcy-Weisbach.

The simulated and experimental velocities at 9.9 m downstream of the box tank are presented in Fig. 3.4. The model predictions and experiments for the pressure head at 14.1 m downstream of the box tank are presented in Fig. 3.5. The simulated results were generated using 400 cells and a Cr of 0.80. The results for the velocities (Fig. 3.4) show a good agreement between model and experiments for the frequency of oscillations. However, the velocity amplitudes are overestimated by the model. As suggested by Vasconcelos et al. (2006), this may be in part because the outflow uniformity assumption which may not be accurate. The differences between model prediction and experiments may be associated also to neglecting unsteady friction in the model. As can be seen

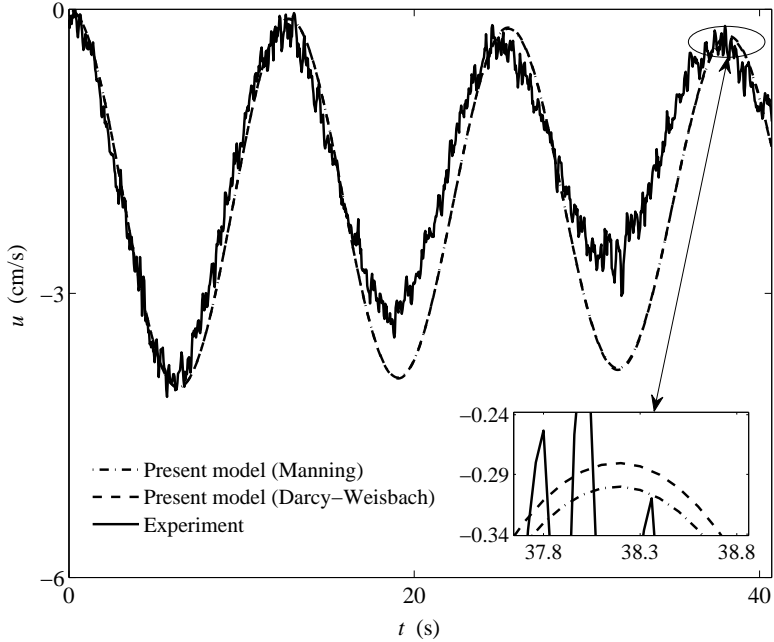


Figure 3.4: Measured and computed velocities at 9.9 m from the upstream end for experiments of Vasconcelos et al. (2006).

in Fig. 3.4, the simulated results using the Manning's and Darcy-Weisbach equation are almost the same, the former being slightly more dissipative. The results for the pressure head (Fig. 3.5) show a good agreement between model predictions and experiments. The differences between the simulated and experimental pressure heads may be explained using the same reasons given for the velocities.

The reason for the oscillations in the velocity (Fig. 3.4) may not be clear at first examination. However, by taking a look at the pressure head plot (Fig. 3.5), the aforementioned oscillations start to make sense. The velocity at a given section is associated with the local difference in pressure head at both sides of the section. In the experiment, the outflow from the upstream tank creates a variation of the pressure head in the whole pipeline. Since both tanks are relatively small and as the system tries to reach steady state, oscillations in the pressure head are produced (Fig. 3.5). The oscillations in the pressure head in turn cause oscillations in the flow velocity.

3.3.3 Hypothetical three-way merging flow

The hypothetical test presented in this section considers a three-way merging flow system that is depicted in Fig. 3.6(a). As shown in Fig. 3.6(a), all pipes have a length of 5 m, the junction pond has a diameter of 1 m, the inflowing pipes (pipes 1 and 2) have both a diameter of 0.5 m and the outflowing pipe (pipe 3) has a diameter of 0.8 m. The Manning's roughness coefficient

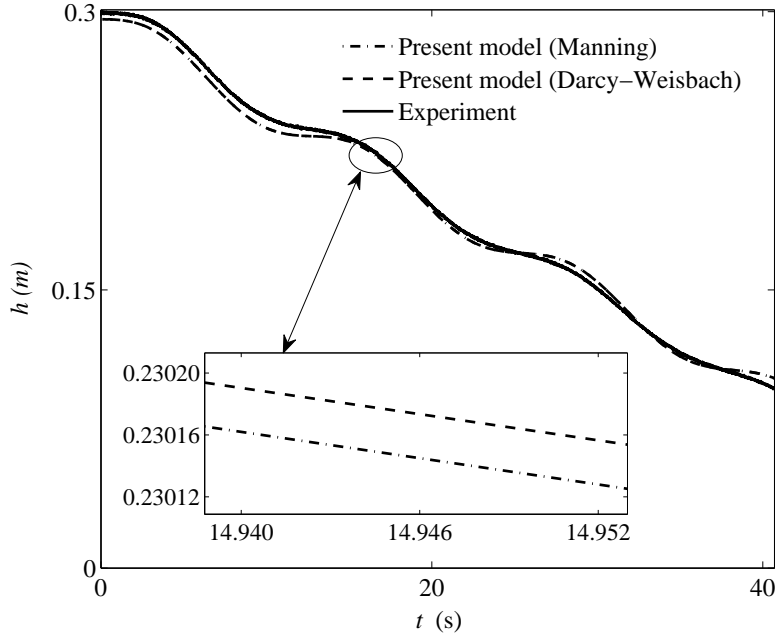


Figure 3.5: Measured and computed pressure heads at 14.1 m from the upstream end for the experiments of Vasconcelos et al. (2006).

used in the 1D simulation is $n_m = 0.015 \text{ m}^{1/6}$, the waterhammer wave speed considered is 100 m/s and the initial flow velocity in all pipes is 0 m/s. A waterhammer wave speed of 100 m/s was used because of PC hard disk storage limitations (200 GB) when running FLOW-3D. For instance when using a mesh of 6,000,000 cells, a pressure wave celerity of 100 m/s, an output time of 0.001 s (to be able to capture the pressure head traces associated with a pressure wave celerity of 100 m/s) and a simulation time of 0.2 seconds, the storage required in the PC was about 150 GB. Given the PC hard disk storage limitations, it was decided to use a maximum pressure wave celerity of 100 m/s in this and the next test case.

It is pointed out that the pressure wave celerity is not a limitation for the ITM model. In fact this model was used for simulating the test case under consideration for pressure wave celerities of 500 and 1000 m/s (results not shown). When using the ITM model, the solutions for free surface flows were identical to those obtained using a celerity of 100 m/s. For pressurized flows, as expected, the amplitude of the pressure peaks were all different from each other, where the largest amplitude was obtained using the highest pressure wave celerity used (1000 m/s).

To ensure that the CFD results (Flow-3D model) are mesh independent a mesh convergence study was performed. This study was performed for the pressure traces at midway of pipe 3 using three mesh sizes, which results are shown in Fig. 3.7. The mesh size used in the study from the smallest to the largest were 797400, 2694465 and 6,000,000 cells, respectively. As can be

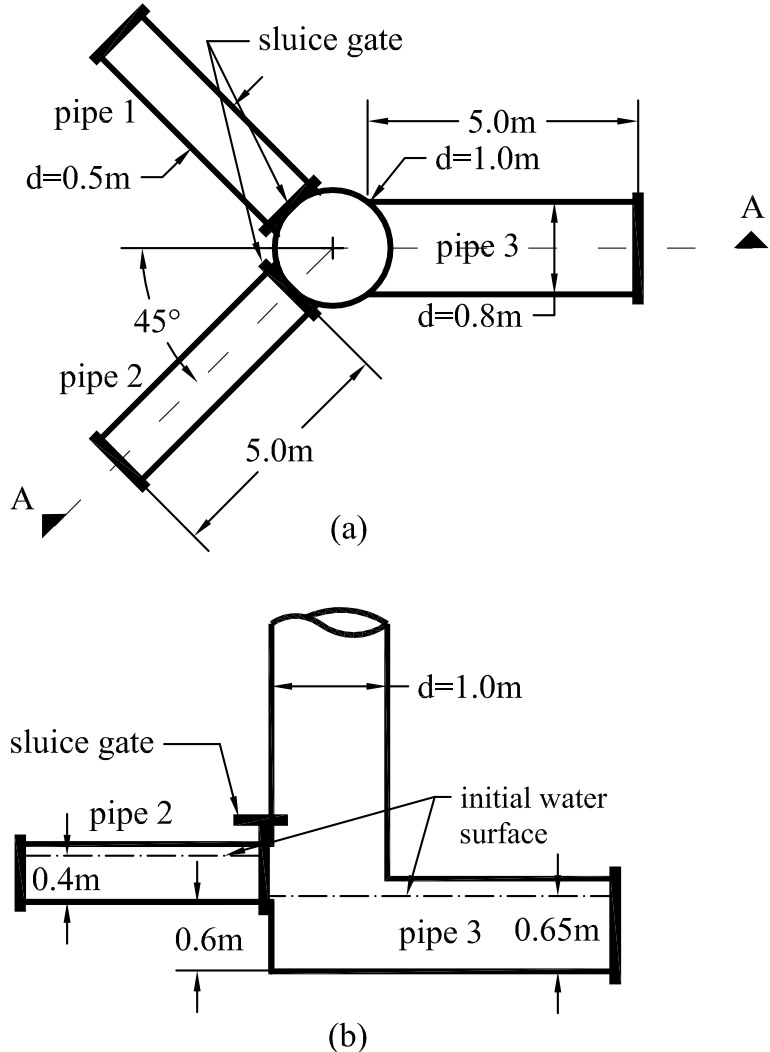


Figure 3.6: (a) Plan and (b) section A-A view for three-way merging flow hypothetical case.

observed in Fig. 3.7, mesh convergence is approximately achieved using the intermediate mesh size (2694465 cells). The CFD results presented in this section and the next one (similar to the present test case) were obtained using a mesh of 6,000,000 cells.

The initial water surface levels for this test are presented in Fig. 3.6(b). As can be observed in Figs. 3.6(a) and 3.6(b), the initial zero-velocity water pools in each pipe are separated by two sluice gates located at the downstream end of each inflowing pipe. The boundary conditions at the upstream end of the inflowing pipes (pipes 1 and 2) and at the downstream end of the outflowing pipe (pipe 3) were assumed to be zero-flux boundaries, which represent a dead-end pipe. The transient flow is obtained after an instantaneous and simultaneous opening of the sluice gates at time $t = 0$.

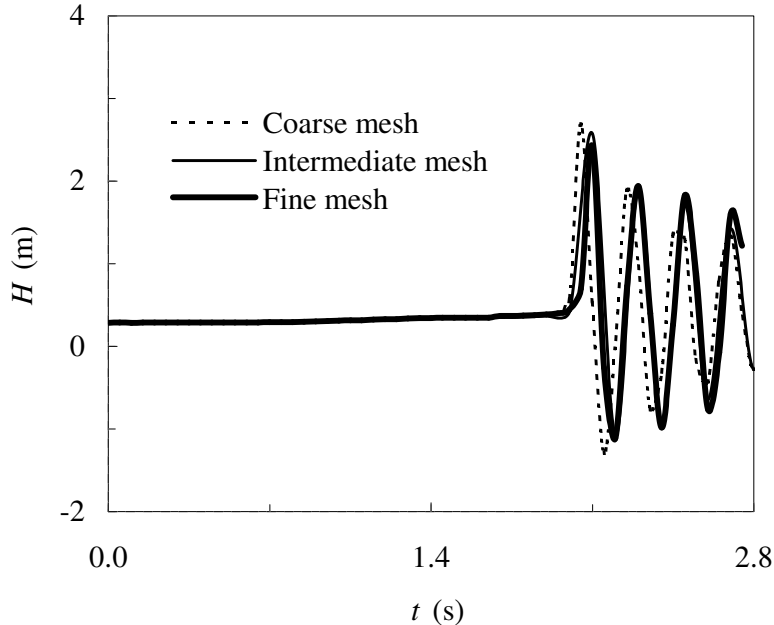


Figure 3.7: CFD mesh convergence for three-way merging flow test case (Pressure head traces at mid-way of pipe 3).

The opening of the sluice gates generated a free surface flow surge at the upstream end of pipe 3 that moved in the downstream direction. The continuous supply from the inflowing pipes into the outflowing pipe (pipe 3) pressurized the upstream end of pipe 3 making the free surface flow surge become an open channel-pressurized flow positive interface that moved in the downstream direction. Once this positive interface reached the downstream end (dead-end) the whole pipe 3 was pressurized and remained that way during the entire simulation. At the inflowing pipes (pipes 1 and 2), the flow remained fully free surface during the entire simulation, although some wave reflections originated at their boundaries (dead-end and junction pond) were observed during the visualization of the simulations. The simulated pressure head traces mid-way of pipes 2 (results for pipe 1 are the same as pipe 2 because of symmetry) and 3 are presented in Figs. 3.8 and 3.9, respectively. The simulation time for this test case was 12 seconds, however for pipe 3 (Fig. 3.9) that involves pressurized flows (high frequency of oscillations) the results are shown only for the first 2.8 seconds for better visualization. The simulated results using the ITM model were obtained using 200 cells in each pipe and a maximum Courant number of $\text{Cr} = 0.8$.

The results of pressure head traces for pipe 2 (Fig. 3.8) obtained using the ITM model agree well with the results obtained using the FLOW-3D model, although the slightly earlier pressurization of the upstream end of pipe 3 when using the ITM model made the free surface flow surge generated at the junction pond arrive earlier at mid way of pipe 2. Fully free surface flow was

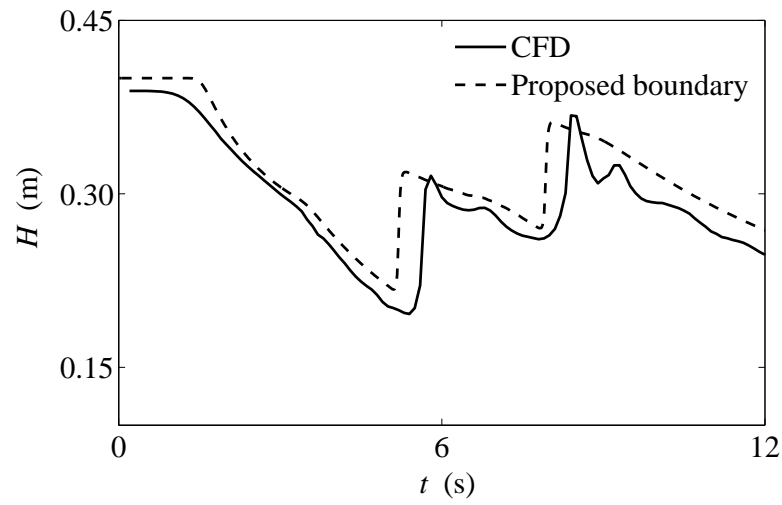


Figure 3.8: Pressure head trace at mid-way of pipe 2.

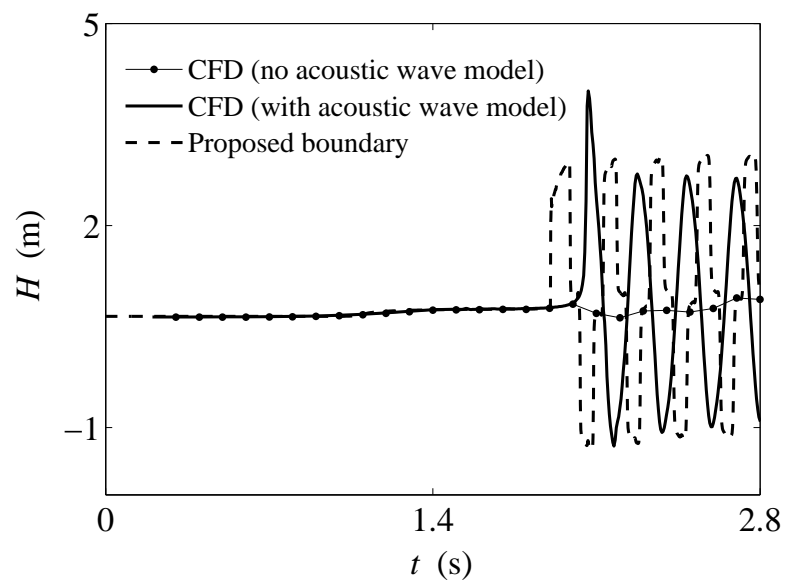


Figure 3.9: Pressure head trace at mid-way of pipe 3.

achieved in pipes 1 and 2 during the entire simulation. The results for pipe 3 (Fig. 3.9), which undergoes a flow type change from free surface flow to mixed flow to pressurized flow, also show good agreement between the ITM model and FLOW-3D (using the acoustic wave model), although this pipe is fully pressurized earlier when using the ITM model. Fig. 3.9 also shows the results of FLOW-3D without using the acoustic wave model. These results show that for pressurized transient flows, the pressure heads obtained without using the acoustic wave model are much smaller than when using this model. The latter results show that the compressibility of the flow (associated with the propagation of acoustic waves) is very important when simulating pressurized transient flows. For simulating free surface flows, considering compressibility of the flow is not important as they produce identical results.

3.3.4 Hypothetical three-way dividing flow

The hypothetical test presented in this section considers a three-way dividing flow system which is depicted in Fig. 3.10(a). As shown in Fig. 3.10(a), all pipes have a length of 5 m, the junction pond has a diameter of 1 m, the inflowing pipe (pipe 1) has a diameter of 0.6 m and the outflowing pipes (pipes 2 and 3) have both a diameter of 0.5 m. The Manning's roughness coefficient used in the 1D simulation is $n_m = 0.015 \text{ m}^{1/6}$, the waterhammer wave speed considered is 100 m/s and the initial flow velocity in all pipes is 0 m/s. A waterhammer wave speed of 100 m/s rather than 1000 m/s was used because of the same reasons as explained in the previous test case. The number of cells used in the CFD simulation was about 6,000,000 and the output time was 0.001 seconds.

The initial water levels for this test are presented in Fig. 3.10(b). As can be seen in Figs. 3.10(a) and 3.10(b), initially the upstream water pool (pipe 1) is separated from the downstream water pools (pipes 2 and 3) by a sluice gate located immediately upstream of the junction pond. The boundary conditions at the upstream end of pipe 1 and at the downstream end of pipes 2 and 3 were assumed to be zero-flux boundaries. The transient flow was produced after an instantaneous opening of the sluice gate at time $t = 0$.

The opening of the sluice gate generated two free surface flow bores at the upstream end of pipes 2 and 3 that moved downstream in the respective pipes. Shortly thereafter, the water supply from the inflowing pipe (pipe 1) into the outflowing pipes (pipes 2 and 3) pressurized and depressurized intermittently the upstream end of pipes 2 and 3 creating positive and negative open channel-pressurized flow interfaces at the upstream end of these pipes. Shortly after, the upstream end of pipes 2 and 3 were fully pressurized, which created positive open channel-pressurized flow interfaces that moved downstream in the respective pipes. Once these positive interfaces reached the downstream end (dead-end) the entire pipes 2 and 3 were pressurized and remained that way during the entire simulation. At the inflowing pipe, the flow remained fully

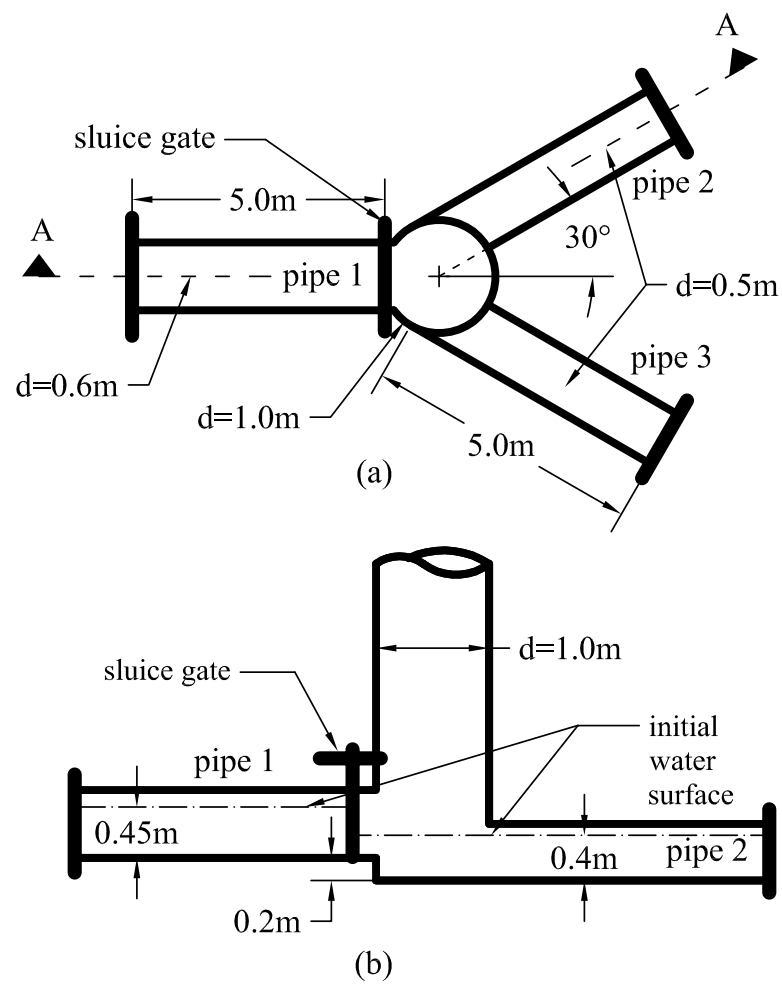


Figure 3.10: (a) Plan and (b) section A-A view for three-way dividing flow hypothetical case.

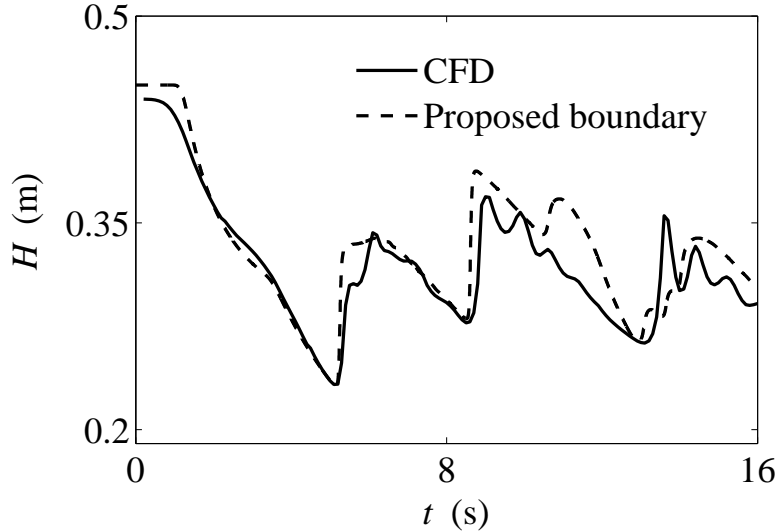


Figure 3.11: Pressure head trace at mid-way of pipe 1.

free surface during the entire simulation, although some wave reflections originating at its boundaries (dead-end and junction pond) were observed during the visualization of the simulations. The simulated pressure head traces midway of pipes 1 and 2 are presented in Figs. 3.11 and 3.12, respectively. The simulation time for this test case was 16 seconds, however for pipes 2 and 3 (Fig. 3.12) that involve pressurized flows the results are shown only for the first 3.6 seconds. The simulated results using the ITM model were obtained using 200 cells in each pipe and a maximum Courant number of $\text{Cr} = 0.8$.

As can be observed in Figs. 3.11 and 3.12, again the agreement between the ITM model and CFD results is good for the frequency and amplitude of free surface and pressurized flow (using acoustic wave model) waves. It is pointed out that the flow in pipes 2 and 3 undergo a flow type change from free surface flow to mixed flow to pressurized flow and in pipe 1 the flow remained fully free surface during the entire simulation. As in the previous test case, for pipes 2 and 3 that involve pressurized transient flows (Fig. 3.12), the pressure heads obtained using FLOW-3D without using the acoustic wave model are much smaller than when using this model. As can be observed in Fig. 3.12, pressure oscillations are simulated using FLOW-3D (with acoustic wave model) between 2 and 2.5 seconds. These oscillations are the result of local pressurization due to fluctuation of free surface flow waves. At about 2.5 seconds, an entire pressurization of pipes 2 and 3 were simulated by the ITM and the FLOW-3D model. The results in Fig. 3.12 also show that the dissipation rate of the pressure waves simulated using the CFD model is slightly faster than the ones simulated using the ITM model.

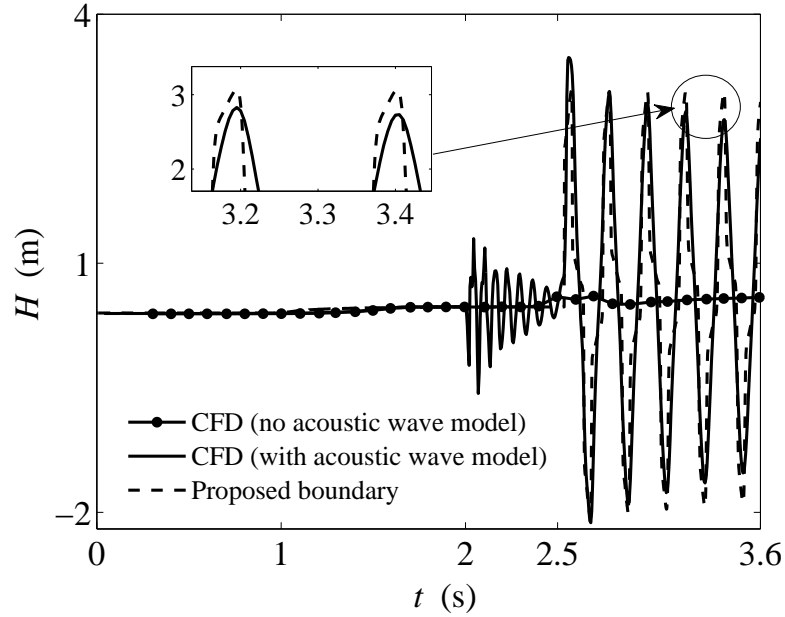


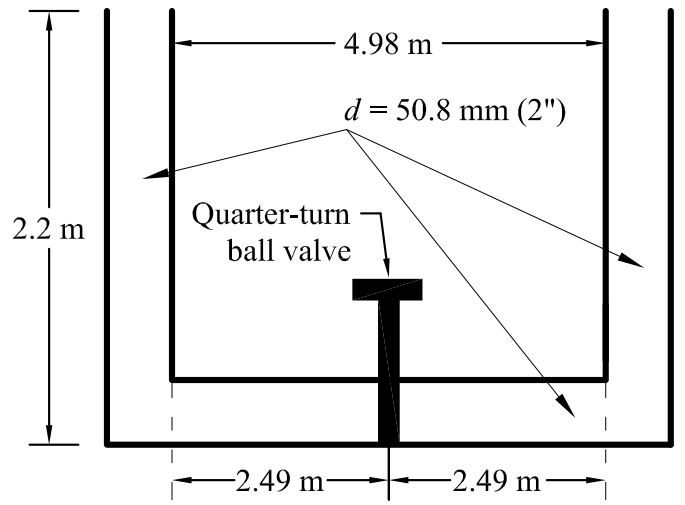
Figure 3.12: Pressure head trace at mid-way of pipe 2.

3.3.5 Experiments of León et al. (2010b) - Oscillation tube

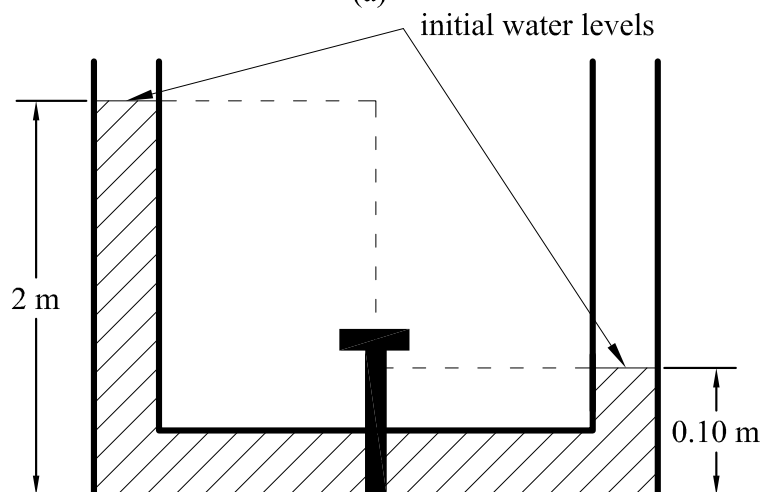
The purpose of this section is to test the ability of the ITM model in simulating pressurized flows in vertical pipes in which water surface level varies rapidly with time. With this purpose, an experimental facility was built in the Ven Te Chow Hydrosystems Laboratory of the University of Illinois at Urbana-Champaign, which layout is depicted in Fig. 3.13 (a). As shown in Fig. 3.13, the experimental setup consisted of a 4.98 m long horizontal plexiglass pipe connected at its upstream and downstream ends by a 2.2 m long vertical pipe of the same material as the horizontal pipe. The inside diameter of all pipes was 50.8 mm (2"). At the center of the horizontal pipe, a quarter-turn ball valve was installed, which as shown in Fig. 3.13 (b), separated the initial water levels upstream and downstream of the valve. The length of the vertical pipes are intentionally chosen to be of the same scale as of the horizontal pipe so that the vertical flow has a clear effect on the results. The water levels in the upstream vertical pipe (left vertical pipe in Fig. 3.13) were recorded using a Canon GL2 color video camera. For a better visualization of the water levels, the water in the oscillation tube was previously dyed. The acquired images were post-processed using the Image Processing Toolbox of MATLAB. For the MATLAB analysis, the video images were converted first to gray-scale images that in turn were converted to black and white images (binary system: 1 = black and 0 = white). The water level for each image was determined by computing the maximum row that has a pixel with a value of 1.

As a frame of comparison for the ITM model, besides laboratory results, CFD (OpenFOAM) modeling results were used. To ensure that the results of the OpenFOAM CFD code are mesh independent a mesh convergence study was performed. This study was performed for the water level elevation at the upstream drop-shaft using three mesh sizes, which results are shown in Fig. 3.14. The mesh size used in the study from the smallest to the largest were 32352, 71100 and 112229 cells, respectively. As can be observed in Fig. 3.14, mesh convergence is achieved using the intermediate mesh size (71100 cells). The CFD results presented in this section were obtained using a mesh of 112229 cells.

The transient flow in the experiments was obtained by a rapid opening of the valve, which created periodic oscillations of water surface levels in the vertical pipes. The measured and simulated water level traces at the upstream vertical pipe (left vertical pipe in Fig. 3.15) are presented in Fig. 3.15. The simulated results using the ITM model were obtained using 400 cells, a pressure wave celerity of 1000 m/s, a Manning roughness coefficient of $0.010\text{ m}^{1/6}$ (typical for a plexiglass pipe), and a Courant number of $\text{Cr} = 0.8$. The results show a good agreement between the ITM, CFD, and measured results for the frequency and amplitude of water level oscillations. The results in Fig. 3.15 labelled “mass/energy” are obtained with the ITM model using the mass and energy equation instead of the mass and momentum equation (used in ITM model). As can be observed in Fig. 3.15, the former approach leads to inaccuracies on the frequency of oscillation of the water surface level. For the accurate prediction of frequency and amplitude of rapid variation of water surface levels in drop-shafts the momentum equation and not the energy equation must be used.



(a)



(b)

Figure 3.13: Experimental setup of León et al. (2010b) (not to scale) (a) dimensions and (b) initial water levels.

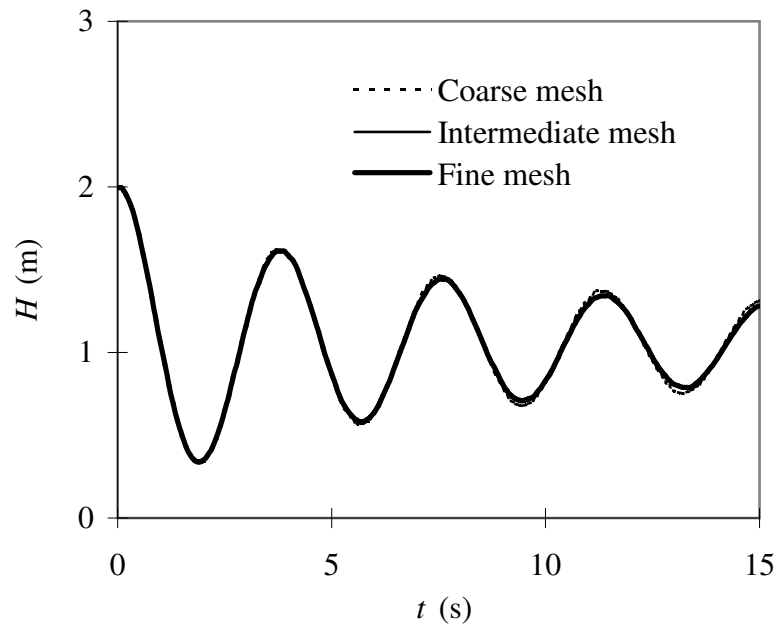


Figure 3.14: CFD mesh convergence for oscillation tube test case (Water level elevation at upstream drop-shaft).

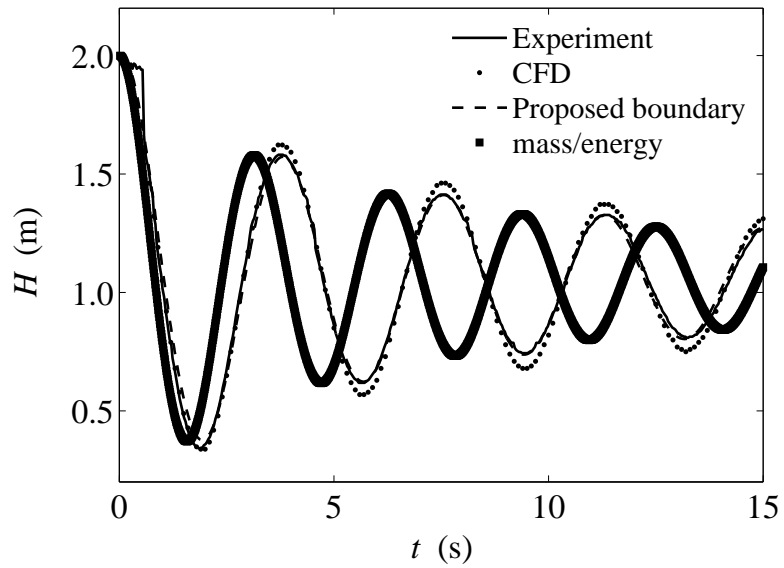


Figure 3.15: Water level elevation at upstream drop-shaft.

Chapter 4

Working with the ITM model

The steps for using the ITM model are:

1. Draw a network representation of the physical components of the closed-conduit system;
2. Add inflow hydrographs;
3. Edit the properties of the objects that make up the system;
4. Specify the set of options for the simulation;
5. Run the simulation; and
6. View the results of the simulation.

As mentioned earlier, the graphical user interface of the ITM model was modified from the graphical user interface of the SWMM model. In this section, only new attributes that are unique to the ITM model are presented. For details of the SWMM model the reader is referred to Rossman (2004).

4.1 Network representation

The network representation of the ITM model is very similar to that of the SWMM model. The network elements supported by ITM are six [conduit elements, junctions, reservoirs, constant boundaries (discharge and pressure head), gates and rating boundary] which graphical representation in the ITM model is depicted in Figure 4.1. Following, the six network elements will be described making emphasis on the new attributes of the ITM model.

4.1.1 Conduits

The graphical editor for a *conduit* element in the ITM model is presented in Figure 4.2. In comparison to the SWMM model, two aspects in this figure

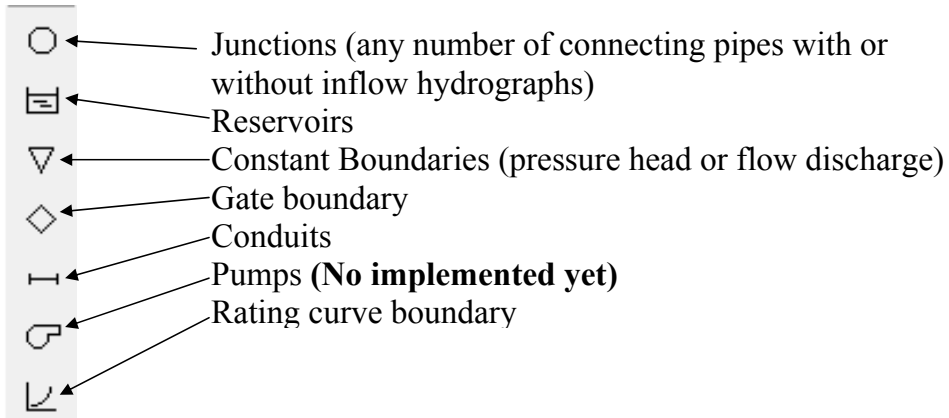


Figure 4.1: Network elements supported by ITM.

need to be commented. The first aspect is that the current version of the ITM model can handle only circular cross-sections. The second aspect is about how to specify the initial flow depth in the system (*initial depth type*). As shown in Figure 4.2, there are three possibilities for defining the initial depth in the conduit, namely, *critical*, *normal* and *constant*. When the option *critical* is selected, ITM will compute the critical depth using the initial flow discharge (*initial flow field* in Figure 4.2) and will assign this critical depth value to all cells of the conduit under edition. Likewise, when the option *normal* is selected, ITM will compute the normal flow depth and will assign this value to all cells of the conduit under edition. When the option *constant* is selected, the ITM model will assign this constant depth to all cells of the conduit under edition.

4.1.2 Junctions

The graphical editor for a *junction* element is presented in Figure 4.3. In comparison to the SWMM model, one aspect in this figure needs to be commented. The ITM model can handle any type of loops with any number of connecting pipes at a junction.

4.1.3 Reservoirs

The graphical editor for a *reservoir* element is presented in Figure 4.4. No inflow hydrographs are allowed at reservoirs, however constant outflows (*Const. outflow* field in Figure 4.4) can be specified at this boundary. The simulation will stop whenever the water depth in the reservoir exceeds the maximum water depth specified in the field *Max. depth*.

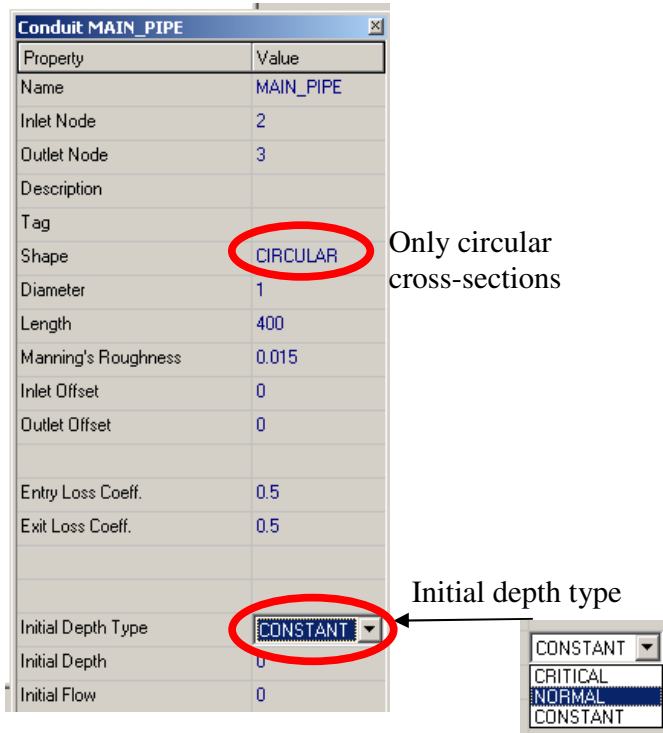


Figure 4.2: Graphical editor for a conduit in ITM.

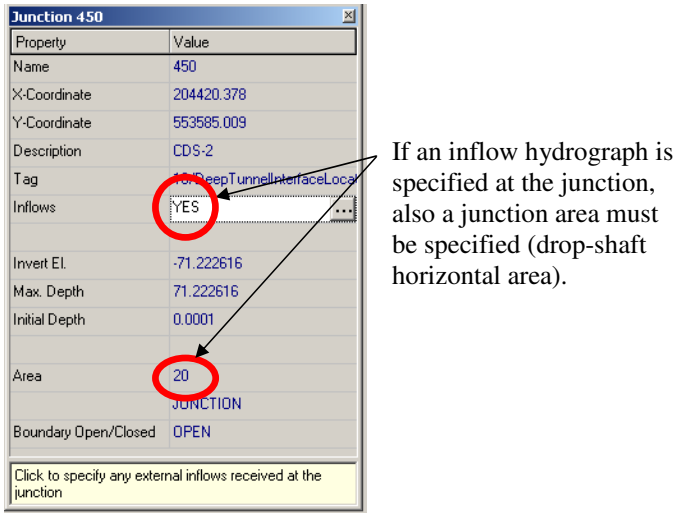


Figure 4.3: Graphical editor for a junction in ITM.

4.1.4 Constant boundaries

The graphical editor for a *constant boundary* element is presented in Figure 4.5. This boundary element can be used *ONLY* when the boundary is connected to *ONE* conduit. In Figure 4.5, three aspects need to be commented. The first

Storage Unit THORNTON	
Property	Value
Name	THORNTON
X-Coordinate	212323.680
Y-Coordinate	546354.000
Description	Thornton Reservoir
Tag	1/TARPJunction
Inflows	NO
Invert El.	-90.678
Max. Depth	89.154
Initial Depth	0.0001
	0
Shape Curve	TABULAR
Const. Outflow	0
Tabular Curve	THORNTON
Curve Name	THORNTON
Constant reservoir outflow (m ³ /s)	

Figure 4.4: Graphical editor for a reservoir in ITM.

aspect is about the field *Boundary Open/Closed*. For this field there are two options, namely *OPEN* and *CLOSED*. The option *CLOSED* must be selected where there is no air ventilation at the boundary (e.g., dead-end tunnel) and *OPEN* when the boundary is ventilated (e.g., lake or river). The second aspect is about the field *Boundary Type*. For this field there are two options, namely, *CONST/FLOW* and *CONST/DEPTH*. The option *CONST/FLOW* must be selected when a constant flow discharge is specified at the boundary. Likewise, the option *CONST/DEPTH* must be selected when a constant depth (or pressure head) is specified at the boundary. For both options (*CONST/FLOW* and *CONST/DEPTH*), the boundary value (flow discharge or pressure head) needs to be specified in the field *Boundary value*.

4.1.5 Gate boundary

The graphical editor for a *Gate boundary* element is presented in Figure 4.6. As depicted in Figure 4.6, the time series for the gate closure and/or opening and the curve of head loss coefficient versus percentage of gate opening need to be specified. The gate head loss coefficient (k) that needs to be specified is given by

$$k = \frac{1}{C_d^2} \quad (4.1)$$

where C_d is the discharge coefficient.

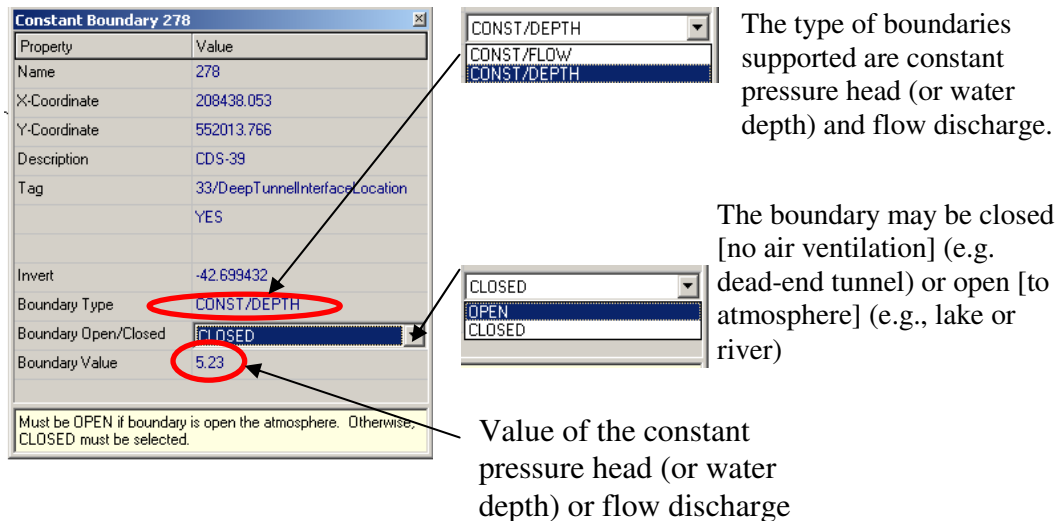


Figure 4.5: Graphical editor for a constant boundary.

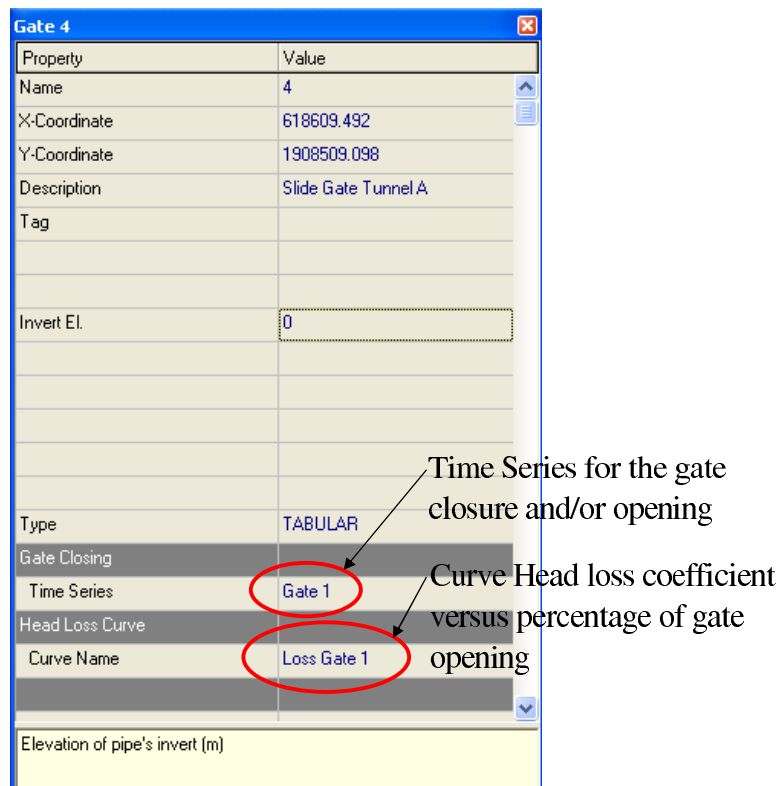


Figure 4.6: Graphical editor for a gate boundary.

4.1.6 Rating curve boundary and Warning

This boundary element can be used to represent weirs, or any other structure that can be represented by a relation of outflow discharge versus pressure

head (Q vs h). The graphical editor for a *Rating curve boundary* element is presented in Figure 4.7.

Warning

Do not use this boundary unless you provide an accurate relation of Q vs h at the rating BC and that the flow at the weir remains always in free surface regime. Otherwise specify a reservoir boundary with bottom elevation below the pipe end invert. ITM will calculate the flow leaving the system, which will enter to the reservoir. You may want to specify a rectangular reservoir for the easy calculation of the flow leaving the system. If the criteria specified above is not satisfied, using a rating BC may mislead the computation of mass in the system and may lead to apparent large errors in conservation of mass. This is because the rating curve BC will likely have convergence problems and the model will assume that the specified amount of water leaves the system, which may be a large amount, when in reality this amount is limited by the water available in the cell adjacent to the rating BC.

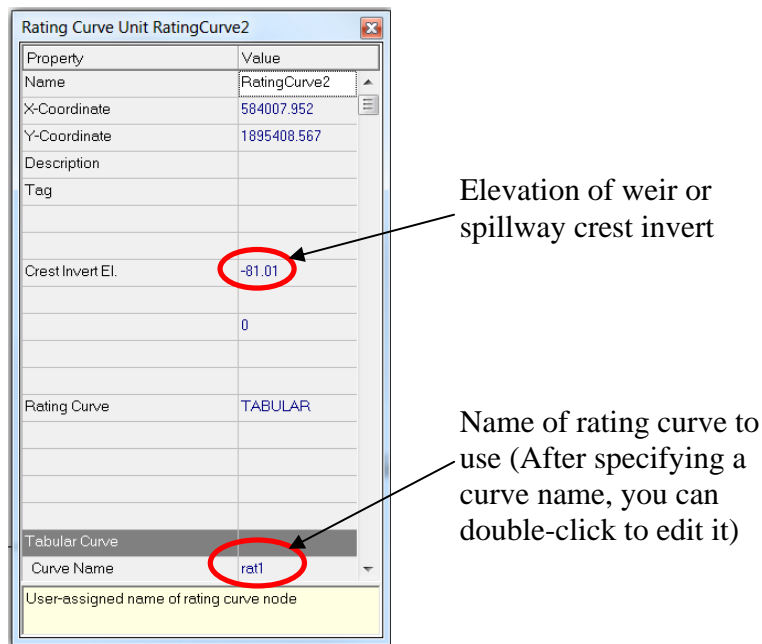


Figure 4.7: Graphical editor for a rating curve boundary.

4.2 ITM Simulation options

The simulation options for the ITM model are presented in Figure 4.8. As can be observed in this Figure, the ITM simulation options has 8 fields, which are described next.

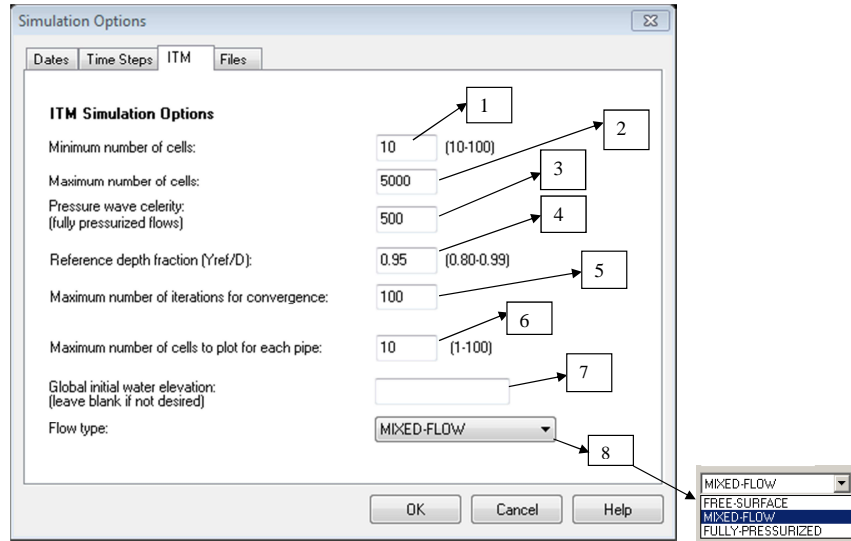


Figure 4.8: Graphical editor for ITM simulation options.

Field 1: Minimum number of grid options: This field refers to the minimum number of cells to be used for the shortest conduit.

Field 2: Maximum number of cells for each pipe: This field refers to the maximum number of cells that can be used in a conduit.

Field 3: Pressure wave celerity (a) : This field refers to the waterhammer wave speed to be used in the simulations.

Field 4: Reference depth fraction: This field refers to the ratio water depth-diameter at which the transition from free surface to pressurized flow is assumed to occur. In mixed flow conditions, this ratio may be set between 0.80 and 0.99. For fully-pressurized flows, this ratio can be set equal to 1.0.

Field 5: Maximum number of iterations for convergence: This field refers to the maximum number of iterations to be used in the ITM model when solving iterative equations (e.g., non-linear system of equations).

Field 6: Maximum number of cells to plot for each pipe: This field refers to the maximum number of cells to be used for plotting (and storing) the pressure head at each pipe.

Field 7: Global initial water elevation (leave blank if not desired): If initially the entire or part of the system is subjected to stationary flow conditions (constant water surface level and zero flow velocity) specify in this field the elevation of this water surface level. If the simulation starts from dry-bed conditions leave this field blank.

Field 8: Flow type: This field refers to the flow type of the simulation. This field is used to avoid checks when running the simulation. For instance, if before hand it is known that fully-pressurized flows will be simulated, no checks for depressurization need to be performed at every time step. In the current version, choosing free surface flow or mixed flow makes no difference. This distinction will be added later. If free surface flow is chosen the program will be terminated when the system is first pressurized (pressurization of an internal cell or boundary).

4.3 Volume mass conservation

ITM generates plots for checking conservation of volume in the system. Plots of volume errors in percentage or in cubic meters can be specified in the main window as *TimeSeriesPlot/ObjectCategory/System(VolumeDiffError* or *Volume%Error)*. As illustration, Figs. 4.9 and 4.10 depict system volume errors in percentage and in cubic meters, respectively.

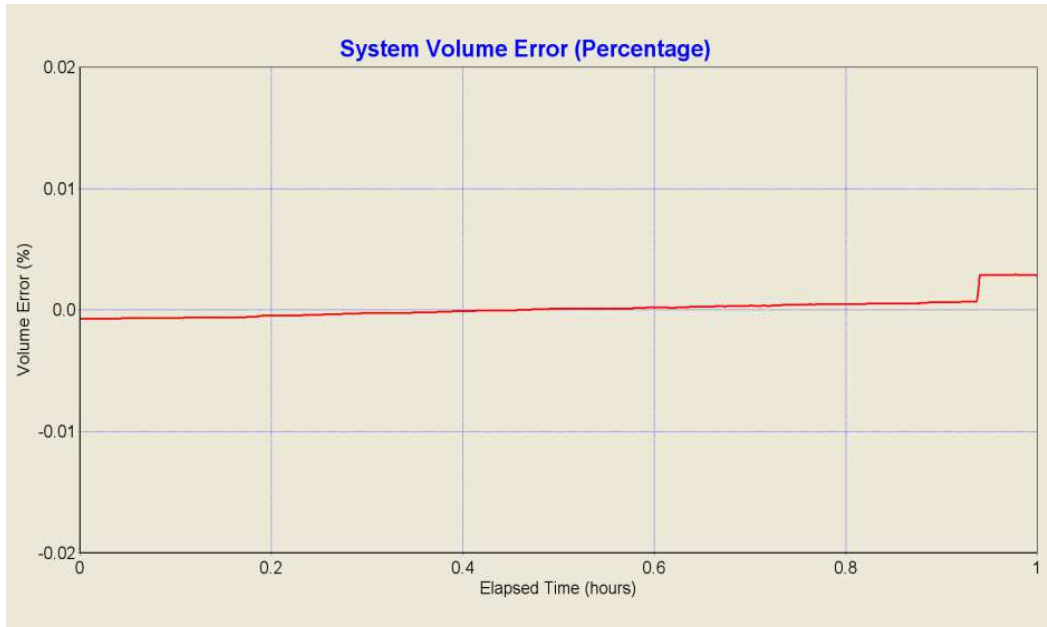


Figure 4.9: System volume error (%).

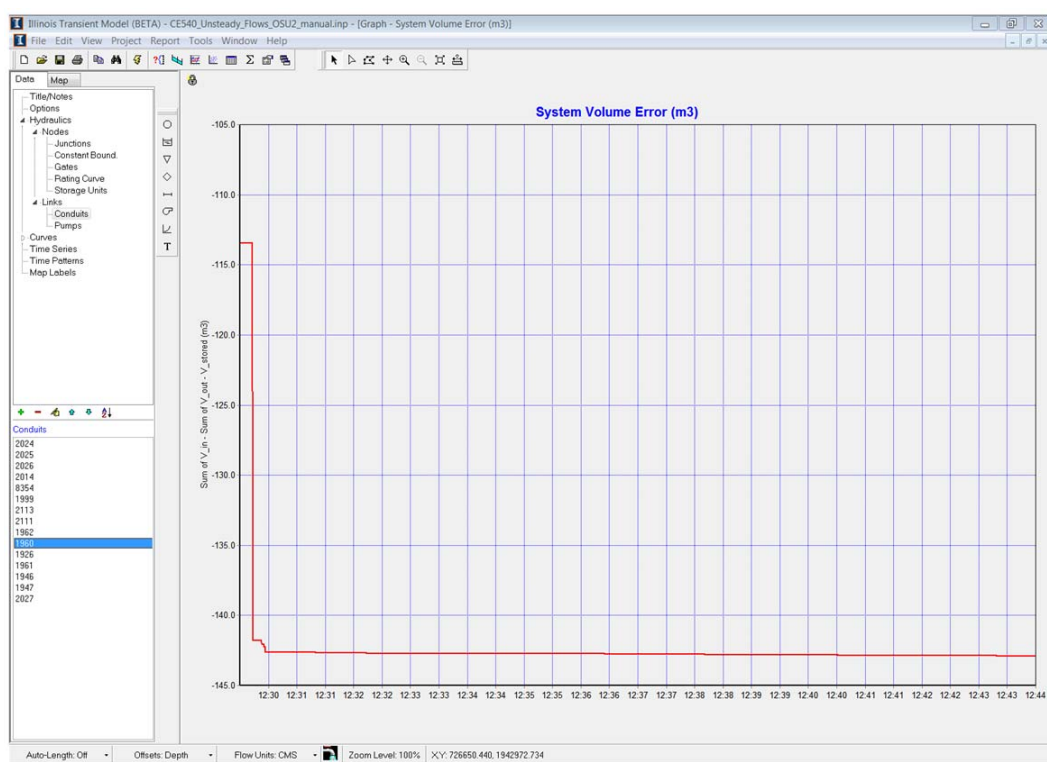


Figure 4.10: System volume error (m^3).

Chapter 5

ITM Examples

In this section, ITM is applied to a hypothetical closed-conduit system to guide its users in setting input data, and running and visualizing results. The hypothetical closed-conduit system, a plan of which is shown in Fig. 5.1, consists of fifteen tunnel reaches, eleven drop shafts with inflow hydrographs, a moving gate boundary at node “gate1”, and a weir at the most downstream end of the system (node “RatingCurve1”) for which a rating curve boundary was specified. An initial dry bed state (zero flow depth and discharge) was used as initial condition. The nodes and conduits (links) of the system are depicted in Figs. 5.1 and 5.2, respectively. Eleven inflow hydrographs were specified for this hypothetical system, one of these is shown in Fig. 5.3. The symbol for an inflow hygrograph in ITM is “H” (see Fig. 5.1).

For the rating curve boundary, data of outflow discharge versus water depth or pressure head (Q vs h) needs to be specified. This is shown in Fig. 5.4 for this example.

For the gate boundary, time series of percentage of gate opening as a function of time and head loss coefficient (k) versus percentage of gate opening need to be specified. These are shown in Figs. 5.5 and Figs. 5.6, respectively. It is recalled that the gate head loss coefficient (k) is given by

$$k = \frac{1}{C_d^2} \quad (5.1)$$

where C_d is the so-called discharge coefficient.

In the current version of ITM all drop-shafts are assumed to have an infinite height. Future experimental and numerical research on overflows will allow a better simulation of the overflows and the return of these flows to the tunnel system. The input files used for this hypothetical system as well as the executable and manuals of ITM are available at the link: <http://web.engr.oregonstate.edu/~leon/ITM.htm>. The input file is located in the same folder as “ITM.exe” under the name “Input files”.

Due to data storage limitations when simulating transient flows, usually different output times are used. A coarse output time is first used to locate the periods at which transients occur in the system. Once the periods of

transients are identified, a fine output time is used but the reporting period is limited to the period of the transients. A fine output time is used to accurately capture the peaks of the pressure oscillations. The dates and time steps in the “simulation options” used for the coarse and fine output times are presented in Figs. 5.7 - 5.10.

When the data storage becomes unmanageable, especially when long periods are simulated, the “HOTSTART” option of ITM may be used. The “HOTSTART” option allows saving the data of the last time step of a simulation and use this data as initial conditions for a new simulation. The interface for setting up the “HOTSTART” option in ITM is presented in Fig. 5.11. To add a HOTSTART file click on *Add*, then enter the name of the HOTSTART file to be created and then select the *Save* button (see Fig. 5.12). To use a HOTSTART file, click on *edit*, then locate the file you want to use and then select the *Use* button (see Fig. 5.13).

The ITM simulation options, which are located within the “simulation options” component, contain the parameters used for the pressure wave celerity, and those that define the accuracy of the simulation. Fig. 5.14 shows the ITM options used in this example. As can be seen in Fig. 5.14, the pressure wave celerity in this example was set to 200 m/s.

As mentioned earlier, the user interface of ITM was modified from the user interface of the SWMM model and it has inherited many of the SWMM features. ITM (in a similar way to the SWMM model) can plot pressure heads (piezometric elevation) and piezometric depths (measured from pipe invert) at any node, and piezometric depth, velocity and flow discharge traces at any conduit or link. **The values reported in ITM for the conduits (i.e., links) are those at their center and not the averages as SWMM.**

The simulation results for the piezometric depth, velocity and flow discharge traces at the center of various conduits (links) for the coarse output time are presented in Figs. 5.15, 5.16 and 5.17, respectively. It is acknowledged that a negative flow discharge or velocity indicates that the flow direction is in opposite direction to the flow in normal conditions (in normal conditions flow is from high to low elevation).

Fig. 5.15 (plot of piezometric depth traces at various conduits) shows several regions of transients. A zoom-in of these regions shows that the peaks and frequency of the pressure oscillations are not well captured. This is because a coarse output time was used for this simulation. For accurately capturing the pressure transients in region A in Fig. 5.15, a fine output time was used for this region. The simulation results for the piezometric depth for region A in Fig. 5.15 (fine output time) are shown in Fig. 5.18.

In the same way as SWMM, ITM can generate plots of two variables at any link or node. For instance the plot of depth versus flow discharge (rating curve) for the link 2026 is shown in Fig. 5.19. This figure clearly shows that a rating curve for pressurized flows in transient conditions does not follow the typical rating curve of open channel flows. ITM also generates user-defined tables and

a text report that summarizes the results of the simulation. As illustration, a typical user-defined table and a typical text report are presented in Figs. 5.20 and 5.21, respectively.

ITM can also generate animations for hydraulic grade lines between any two nodes of the system. The plotting resolution in ITM (number of cells per link or reach) is chosen by the user. As illustration, Figs. 5.22 - 5.25 present hydraulic grade line snapshots between nodes DS15 and RatingCurve1 at different times. These plots can help to visualize the flow dynamics in the system. These plots may also help to identify visually the regions of overflow (when pressure head exceeds terrain level).

ITM also generates the text file “<name of input file>.INP.debug” that is intended for debugging errors. A snapshot of this text file is shown in Fig. 5.26. This file is created in the same folder location to that of the input file.

Finally, ITM generates plots for checking conservation of volume in the system. Plots of volume errors in percentage or in cubic meters can be specified. These plots are obtained using the *Time Series Plot* option as shown in Fig. 5.27. For this example, Figs. 5.28 and 5.29 show the system volume errors in percentage and in cubic meters, respectively.

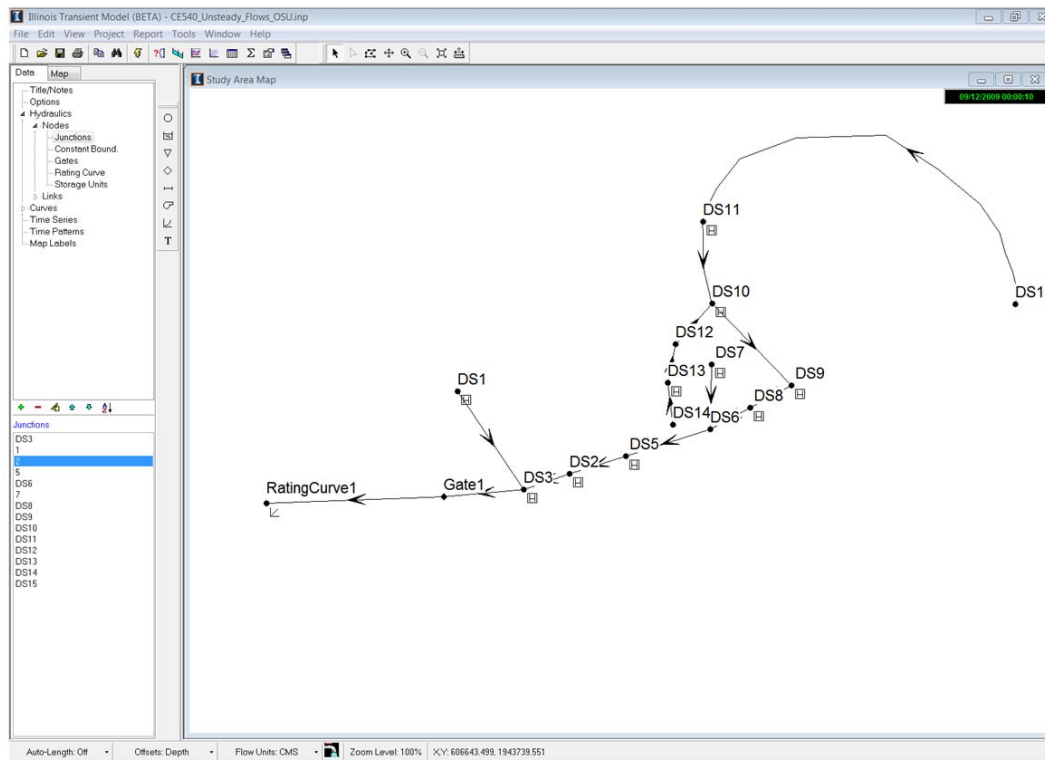


Figure 5.1: Layout of the hypothetical system showing the nodes.

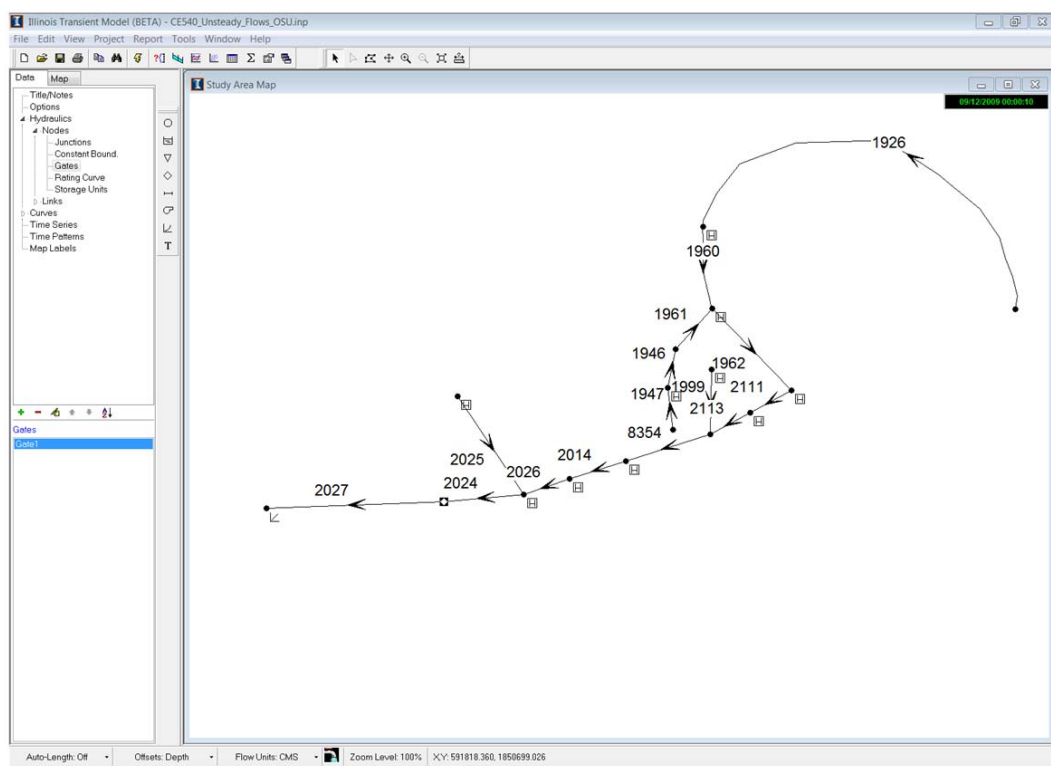


Figure 5.2: Layout of the hypothetical system showing the conduits or links.

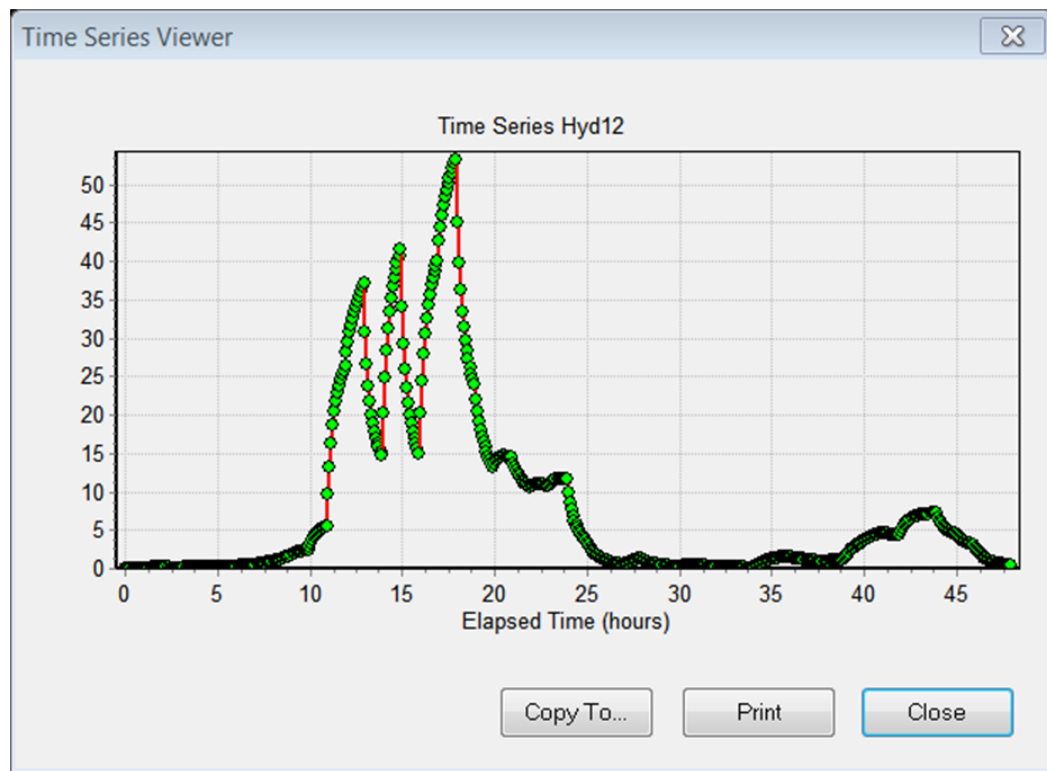


Figure 5.3: One of the inflow hydrographs used for this example.

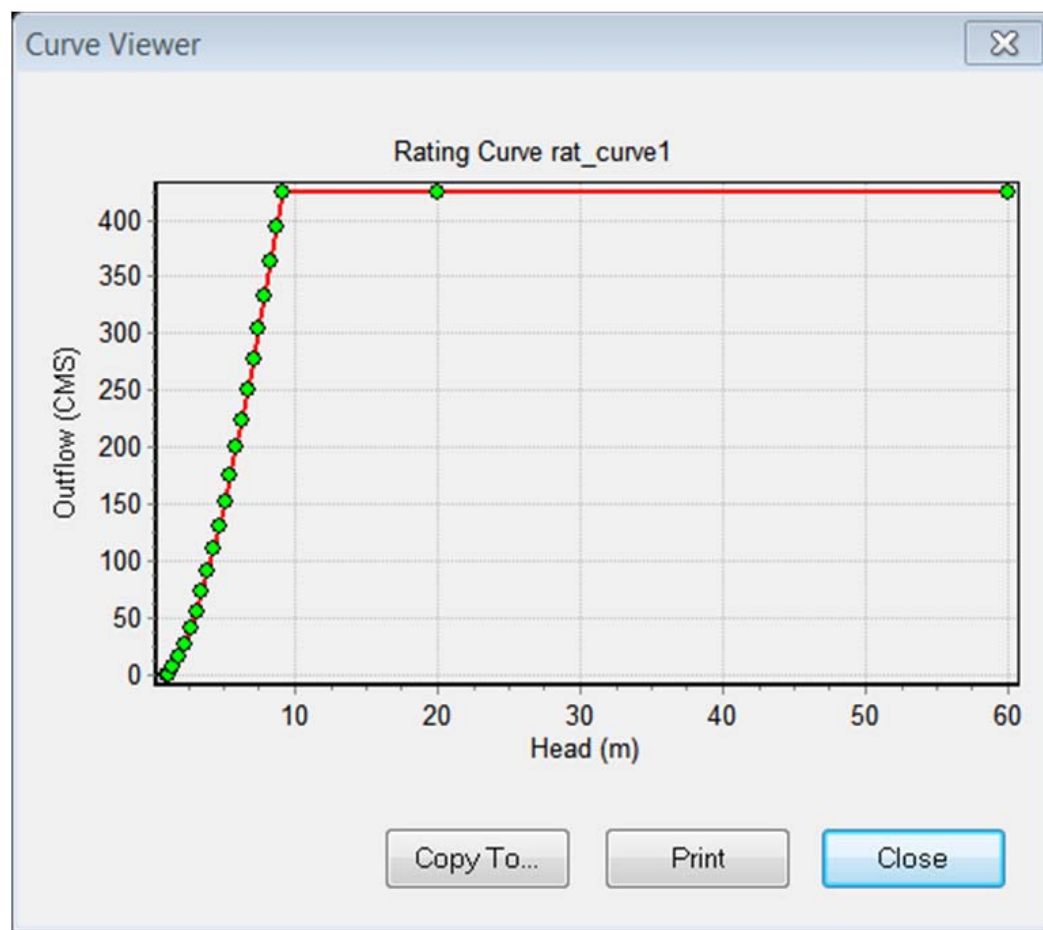


Figure 5.4: Outflow discharge versus water depth for the rating curve boundary.

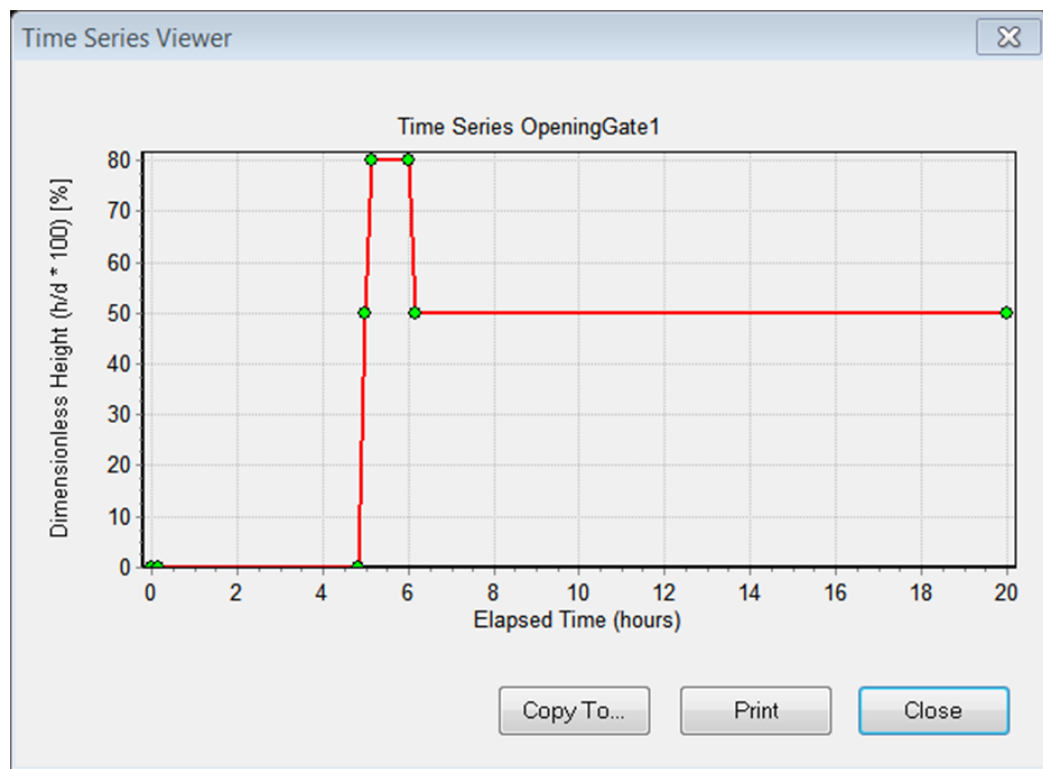


Figure 5.5: Time series of gate opening in percentage.

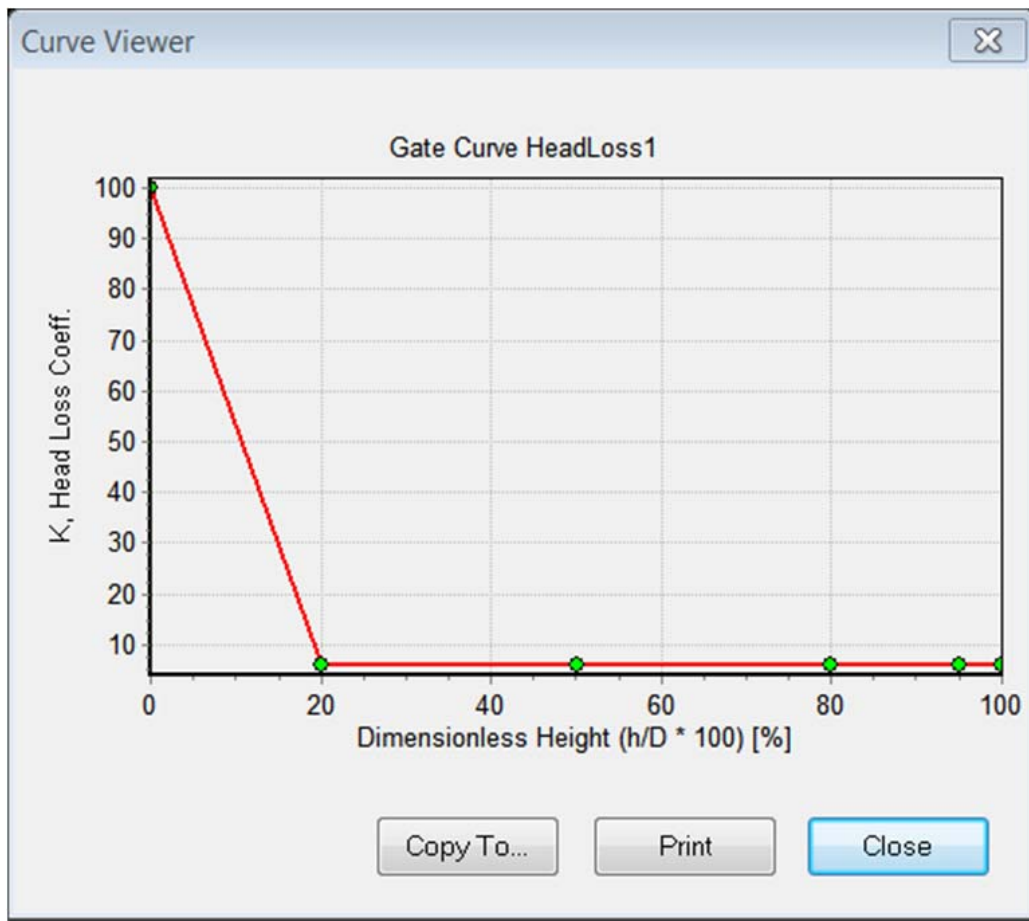


Figure 5.6: Curve of gate head loss coefficient versus gate opening in percentage ($k = 1/C_d^2$, where C_d = discharge coefficient)

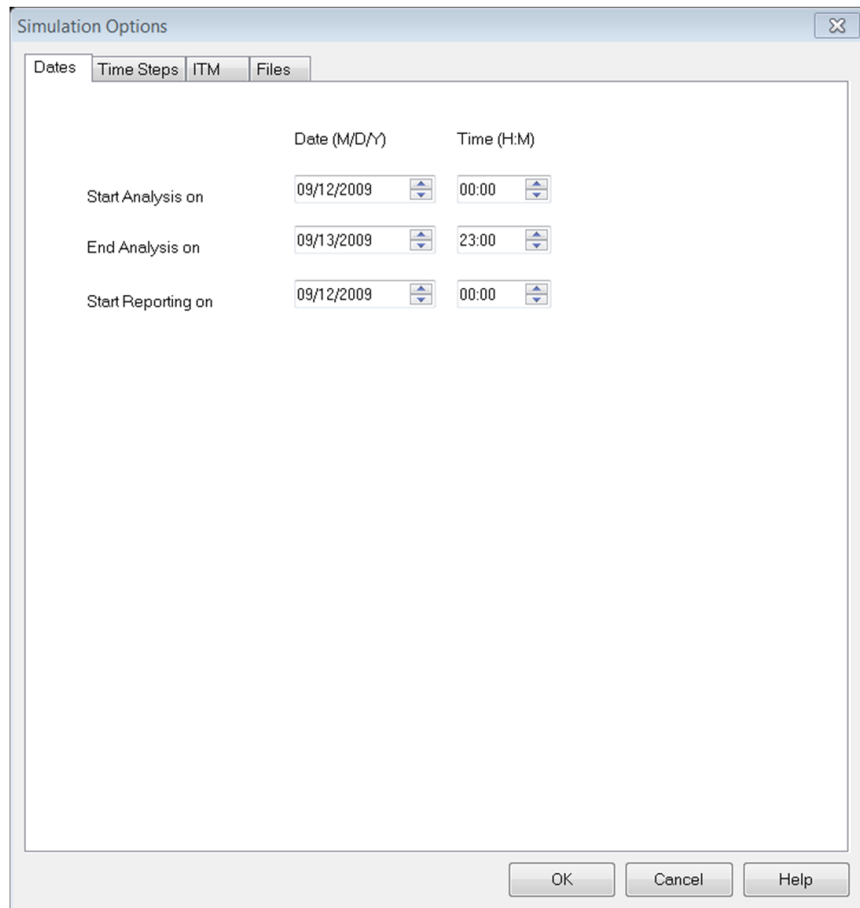


Figure 5.7: Dates in the “Simulation options” for the coarse output time.

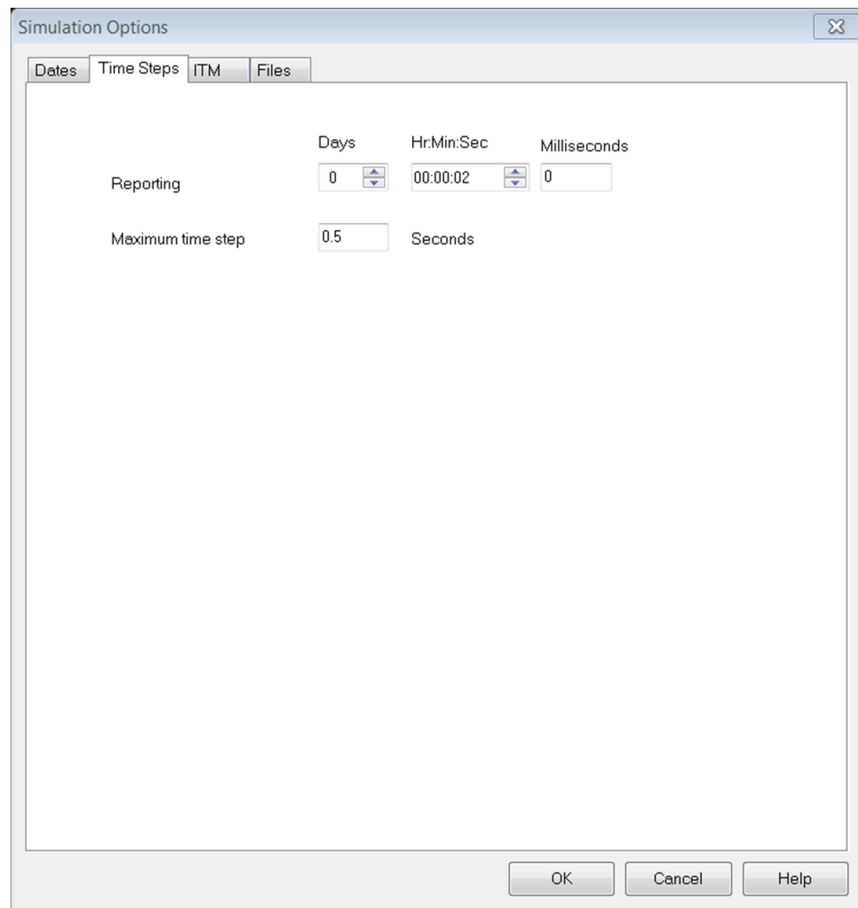


Figure 5.8: Time steps in the “Simulation options” for the coarse output time.

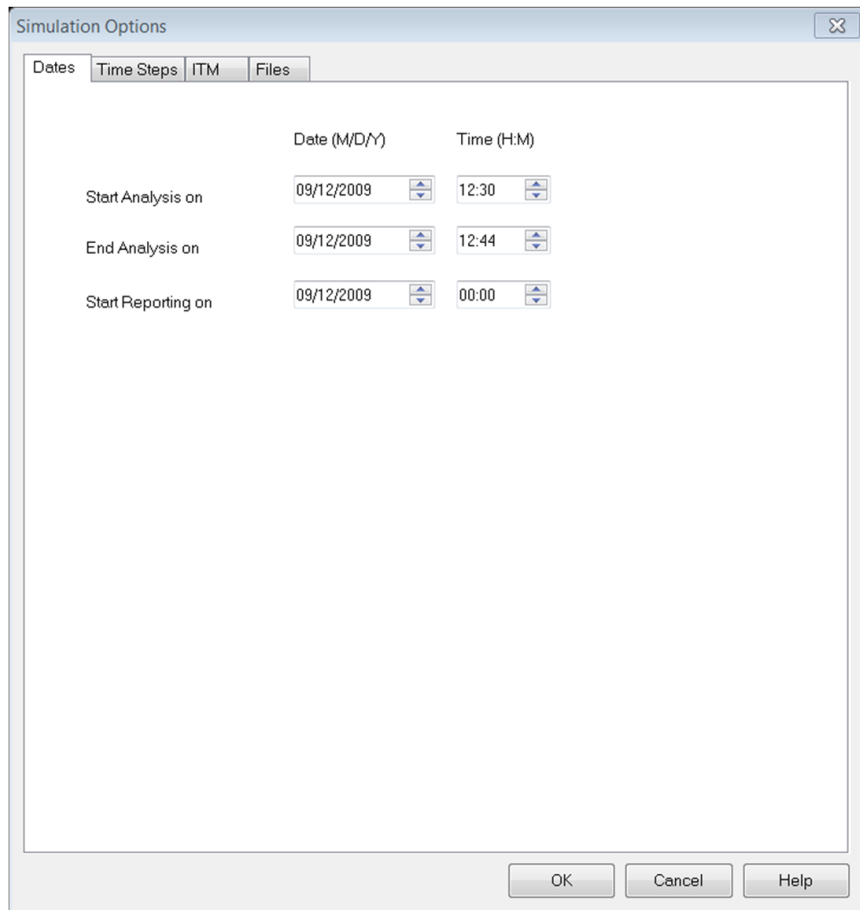


Figure 5.9: Dates in the “Simulation options” for the fine output time.

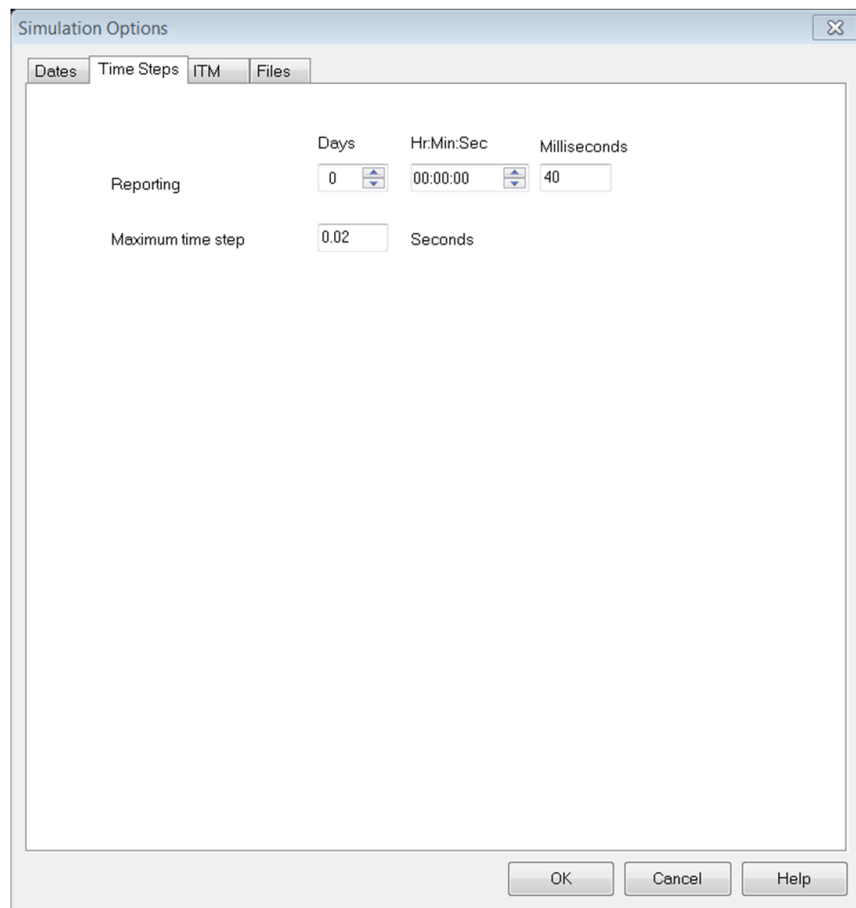


Figure 5.10: Time steps in the “Simulation options” for the fine output time.

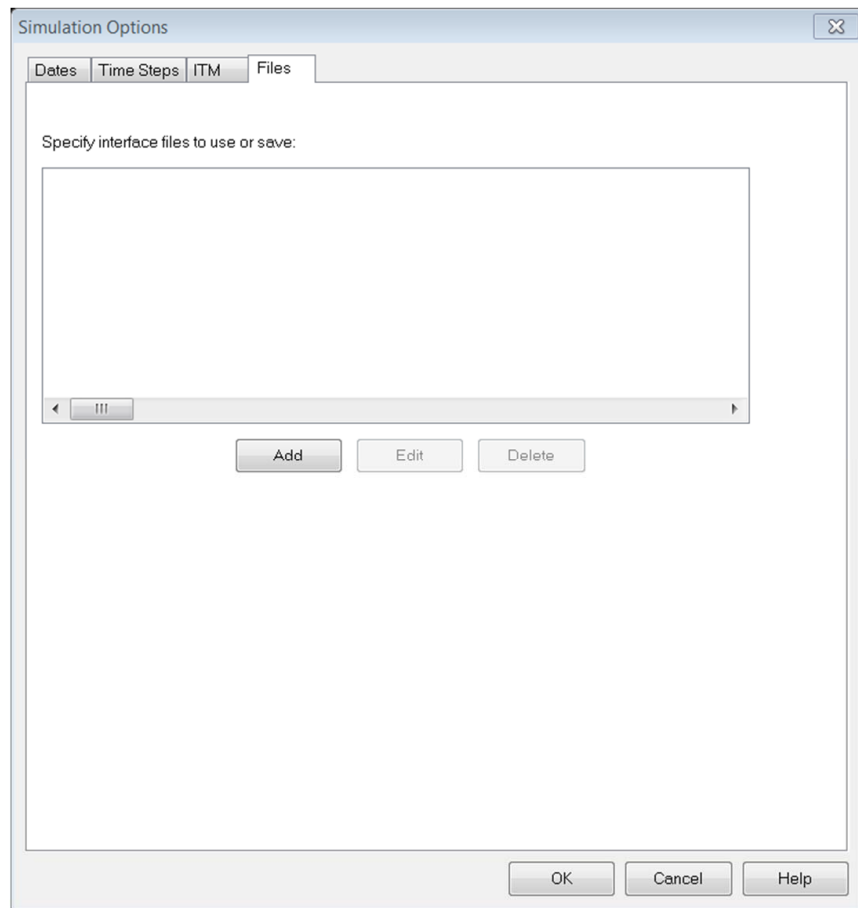


Figure 5.11: Interface for setting up the HOTSTART option in ITM.

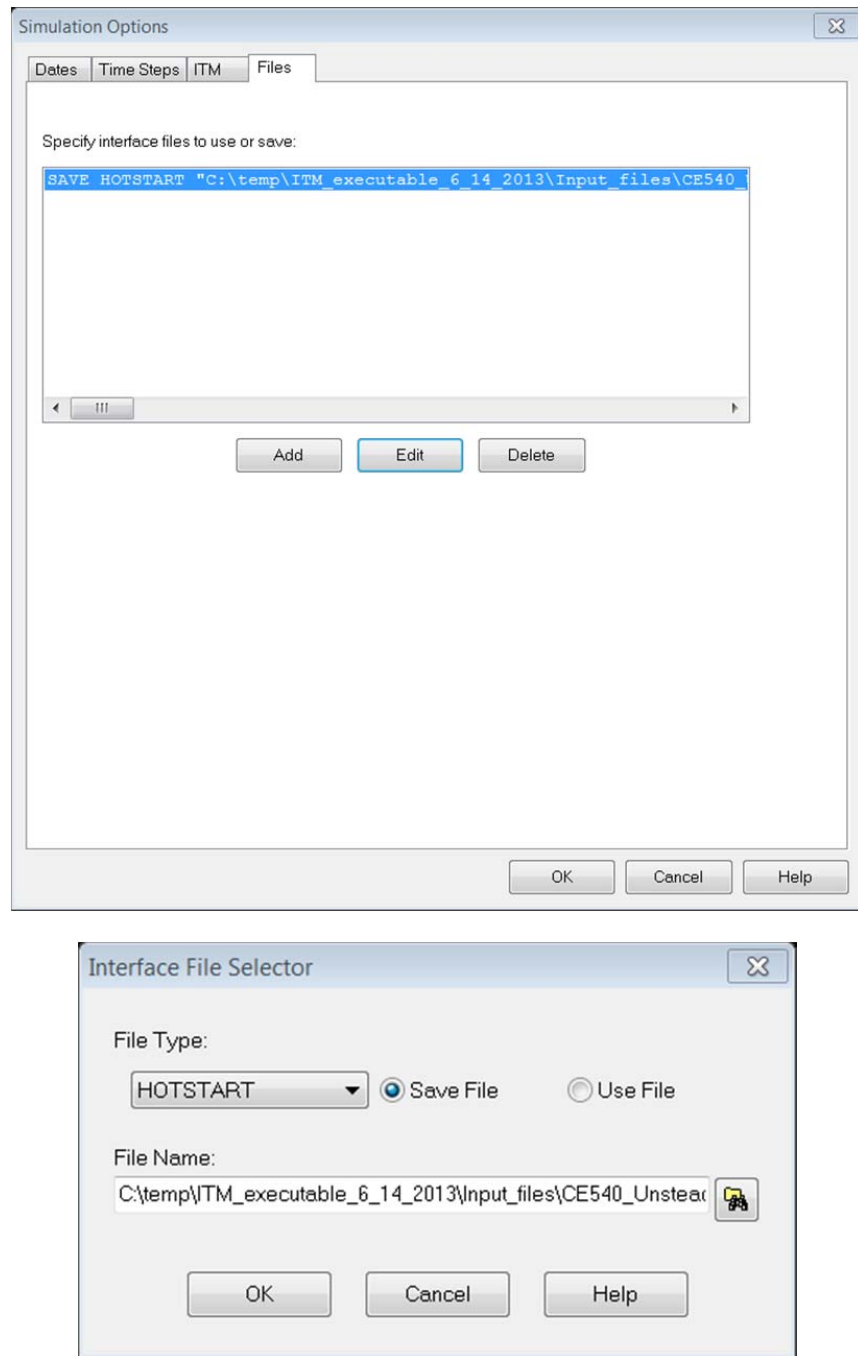


Figure 5.12: Interface for saving HOTSTART file.

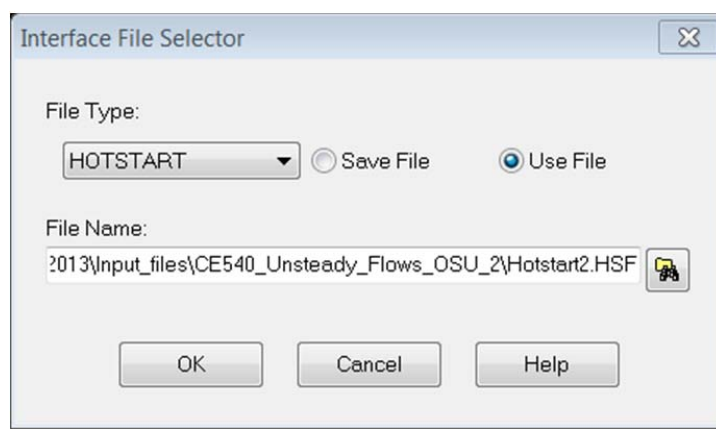
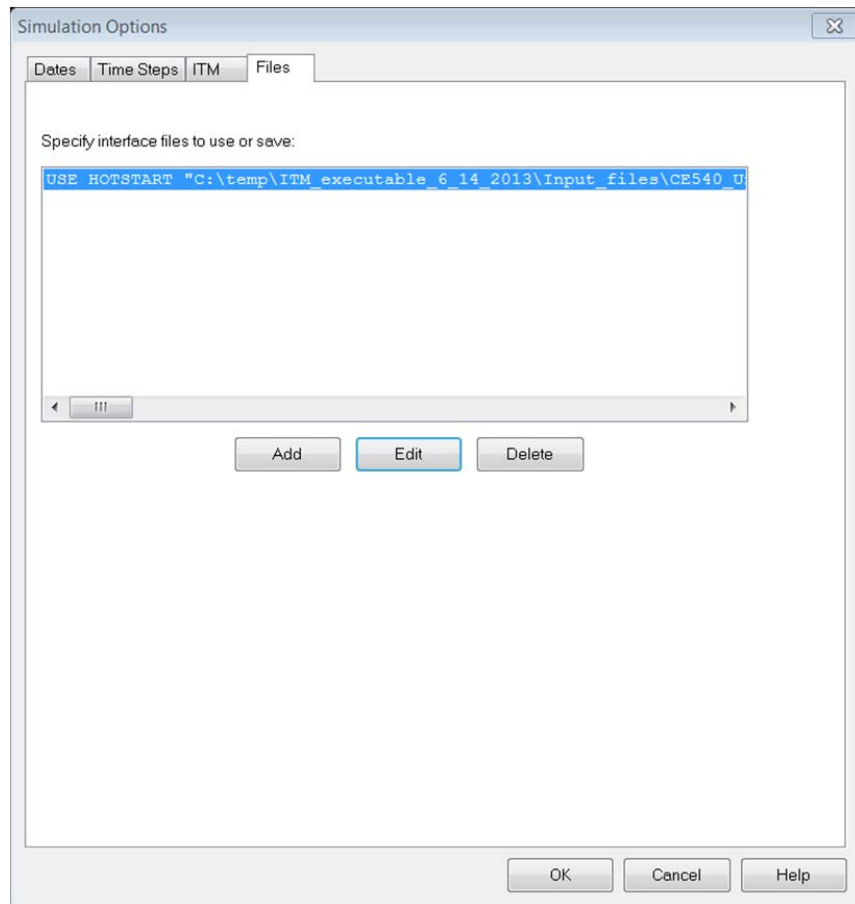


Figure 5.13: Interface for using HOTSTART file in new simulation.

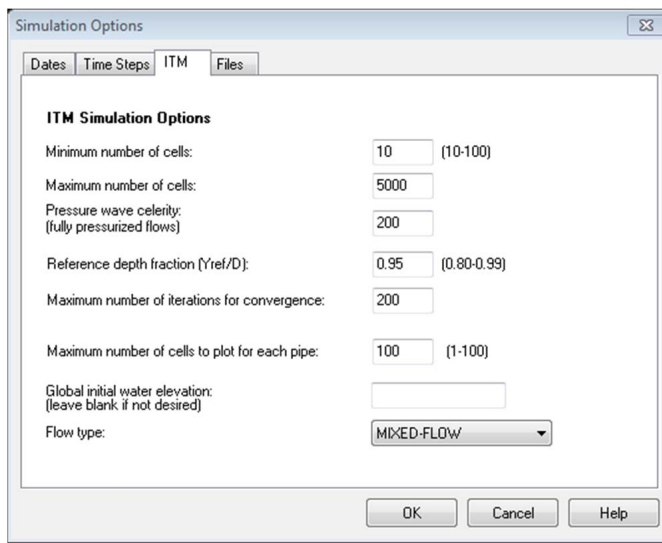


Figure 5.14: ITM parameters in the “Simulation options”.

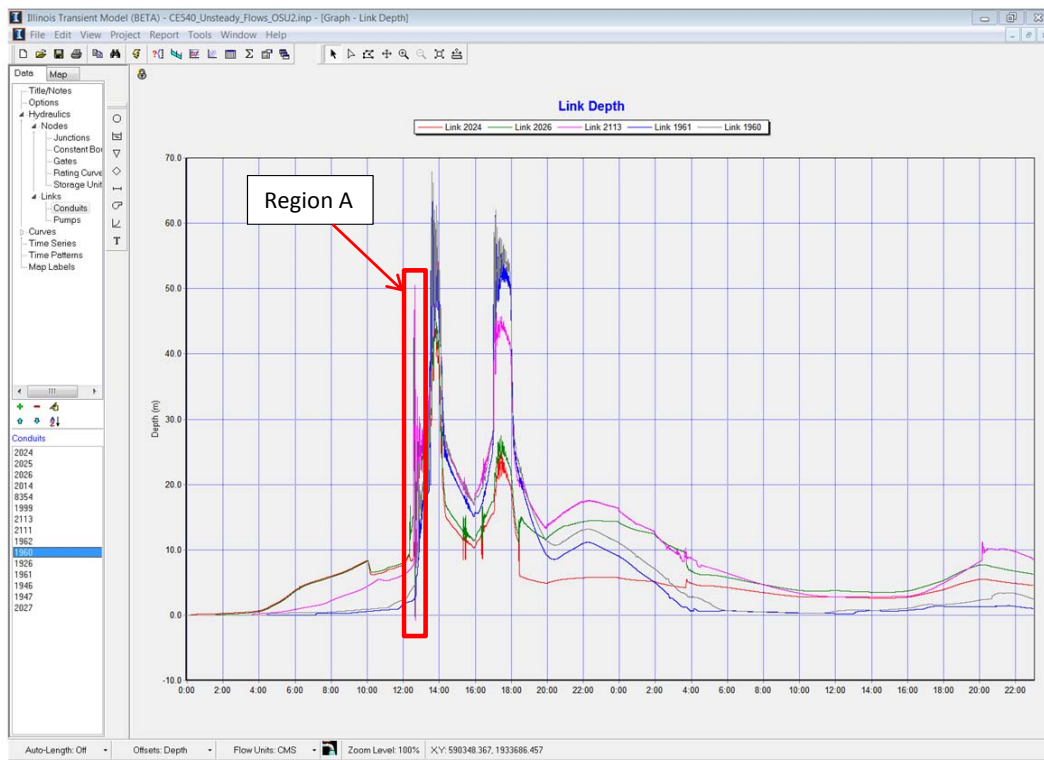


Figure 5.15: Piezometric depth traces at the center of various tunnel reaches for the coarse output time (Initial dry bed state, $a = 200 \text{ m/s}$).



Figure 5.16: Flow velocity traces at the center of various tunnel reaches for the coarse output time (Initial dry bed state, $a = 200$ m/s).



Figure 5.17: Flow discharge traces at the center of various tunnel reaches for the coarse output time (Initial dry bed state, $a = 200$ m/s).

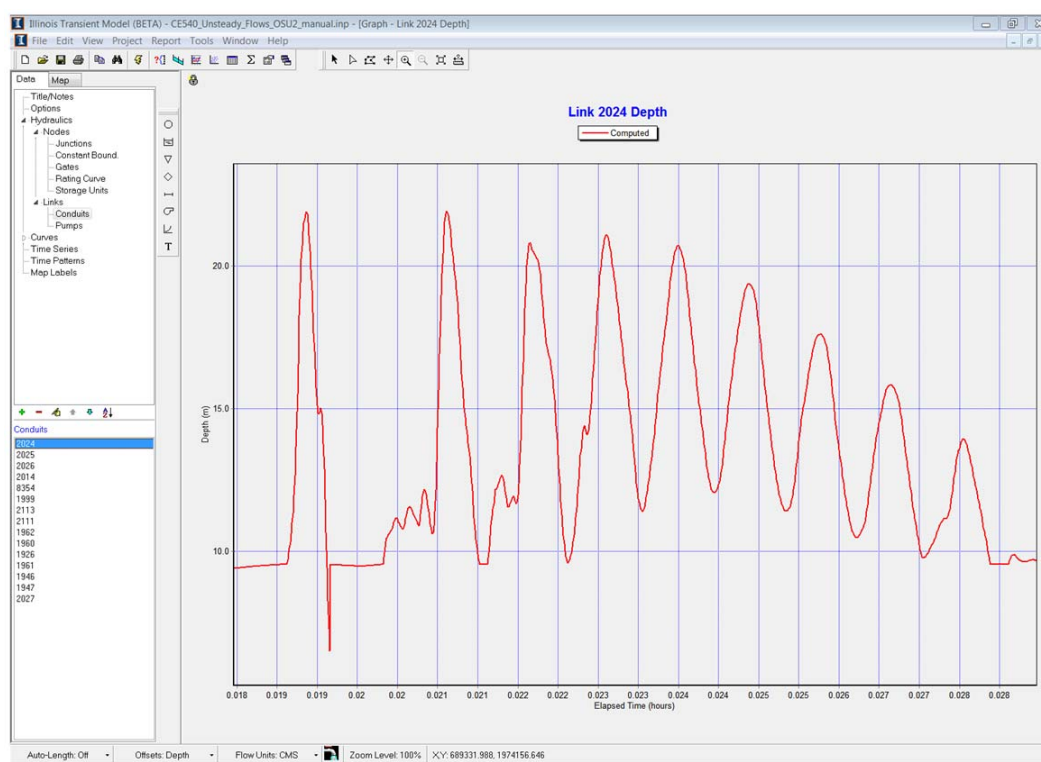


Figure 5.18: Zoom-in of region “A” in Fig. 5.15 using fine output time.

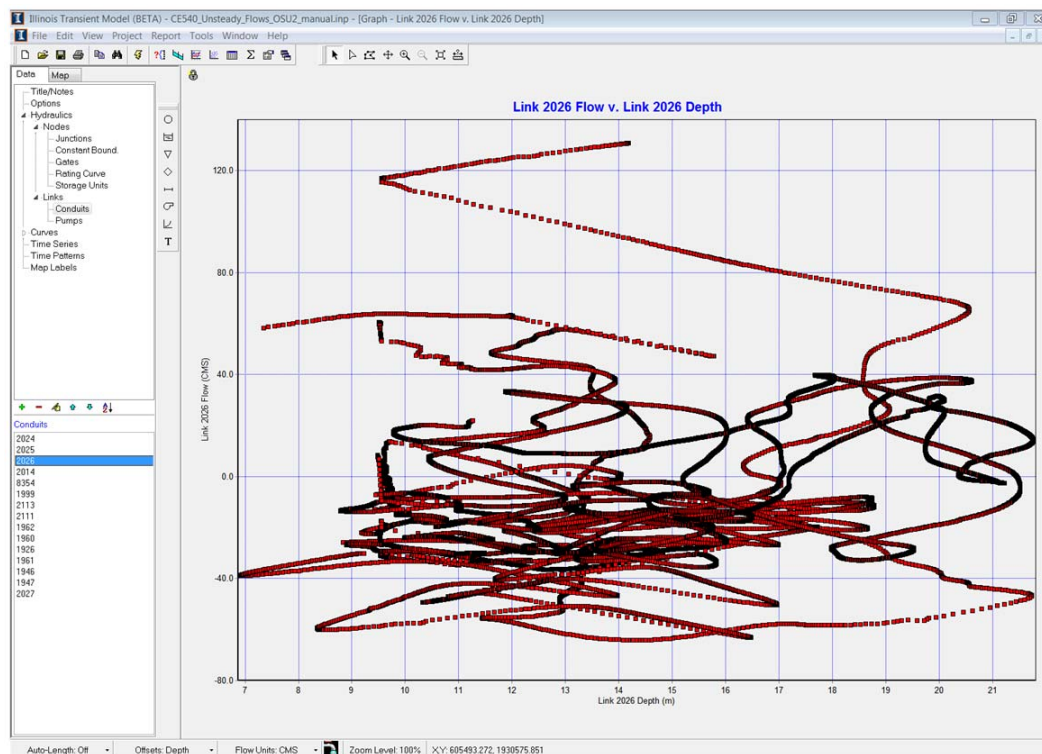


Figure 5.19: Depth versus flow discharge (“rating curve”) for the link 2026 (mid-way of tunnel) (Initial dry bed state, $a = 200$ m/s).

Figure 5.20: Typical user-defined table.

```

ILLINOIS TRANSIENT MODEL - VERSION 1.3 BETA
-----

*****  

Analysis Options  

*****  

Flow Units ..... CMS  

Starting Date ..... SEP-12-2009 00:00:00  

Ending Date ..... SEP-13-2009 23:00:00  

Report Time Step ..... 00:00:02.000  

Maximum Time Step ..... 0.50 sec

*****  

Node Depth Summary  

*****  

-----  

          Average   Maximum   Time of Max  

          Depth     Depth     Depth Occur.  

Node      Type       Meters    Meters   days hr:min  

-----  

DS3       JUNCTION   0.19     46.49    0 13:44  

1         JUNCTION   102.00   13509.31   1 23:00  

2         JUNCTION   0.20     49.57    0 13:47  

5         JUNCTION   0.22     55.26    0 13:46  

DS6       JUNCTION   0.21     57.91    0 13:36  

7         JUNCTION   0.20     59.07    0 13:36  

DS8       JUNCTION   0.22     63.70    0 13:36  

DS9       JUNCTION   0.21     65.64    0 13:40  

DS10      JUNCTION   0.20     67.94    0 13:39  

DS11      JUNCTION   0.13     71.25    0 13:34  

DS12      JUNCTION   0.09     65.18    0 13:38  

DS13      JUNCTION   0.05     57.76    0 13:37  

DS14      JUNCTION   0.01     98.51    0 13:37  

DS15      JUNCTION   0.06     71.06    0 13:39  

Gate1     GATE       0.06     6.33     0 18:27  

RatingCurvel RATINGUNIT 0.07    101.33   0 18:25

*****  

Link Flow Summary  

*****  

-----  

          Maximum   Time of Max  

          Flow     Flow Occur.   Max  

Link      Type       CMS    days hr:min   Depth  

-----  

2024     CONDUIT    445.49   0 17:10    44.05

```

Figure 5.21: Typical text report.

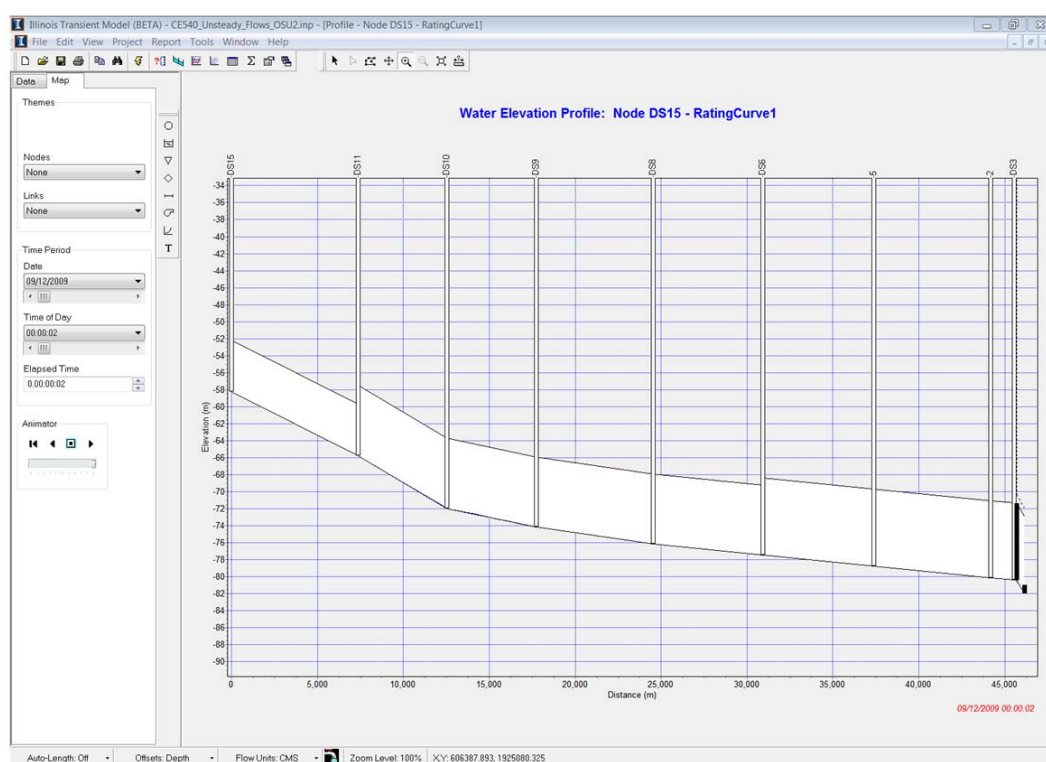


Figure 5.22: Hydraulic grade line snapshot between nodes DS15 and RatingCurve1 after 00 h 00 min 02 sec (Initial dry bed state, $a = 200$ m/s).

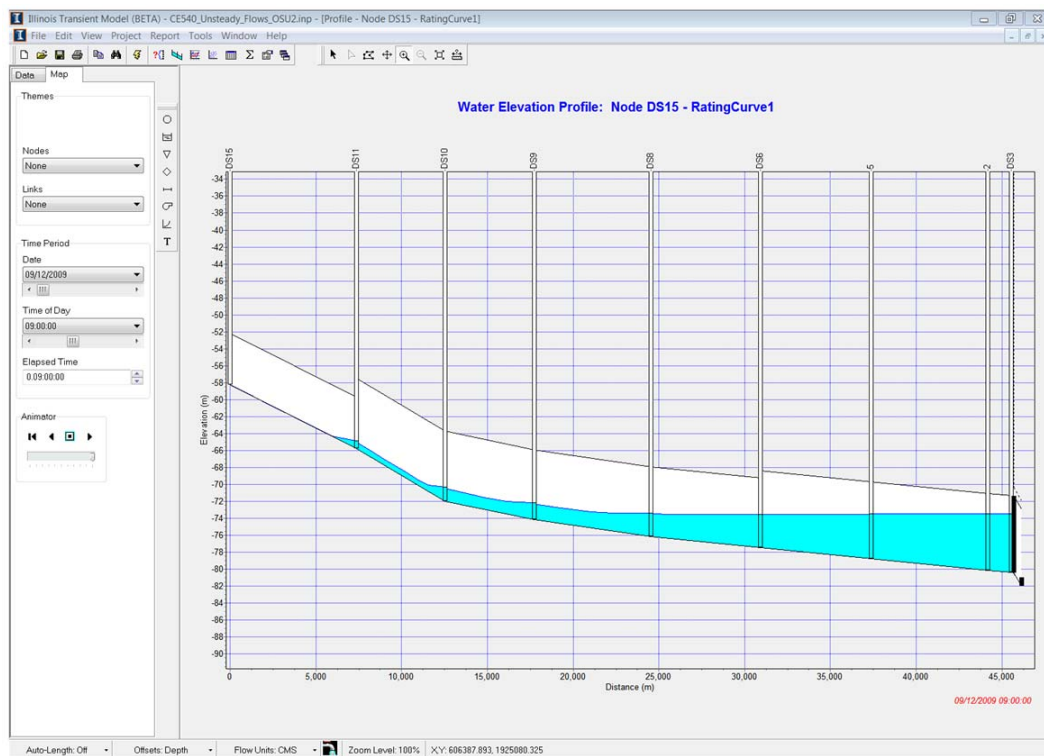


Figure 5.23: Hydraulic grade line snapshot between nodes DS15 and RatingCurve1 after 09 h 00 min 00 sec (Initial dry bed state, $a = 200 \text{ m/s}$).

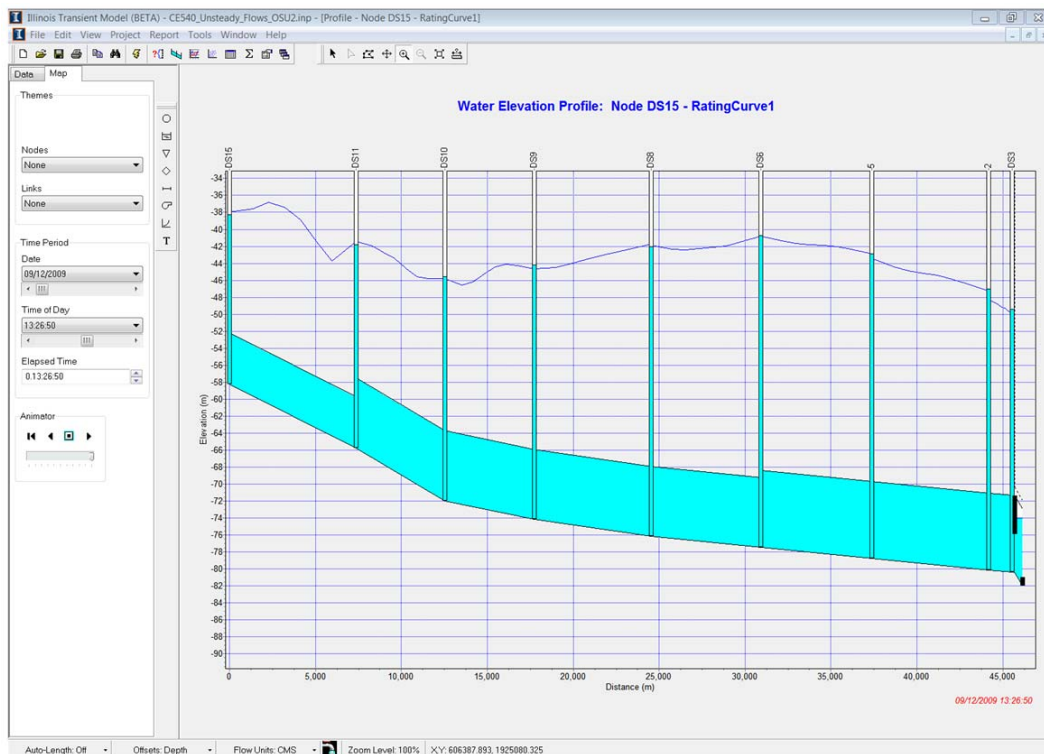


Figure 5.24: Hydraulic grade line snapshot between nodes DS15 and RatingCurve1 after 13 h 26 min 50 sec (Initial dry bed state, $a = 200 \text{ m/s}$).

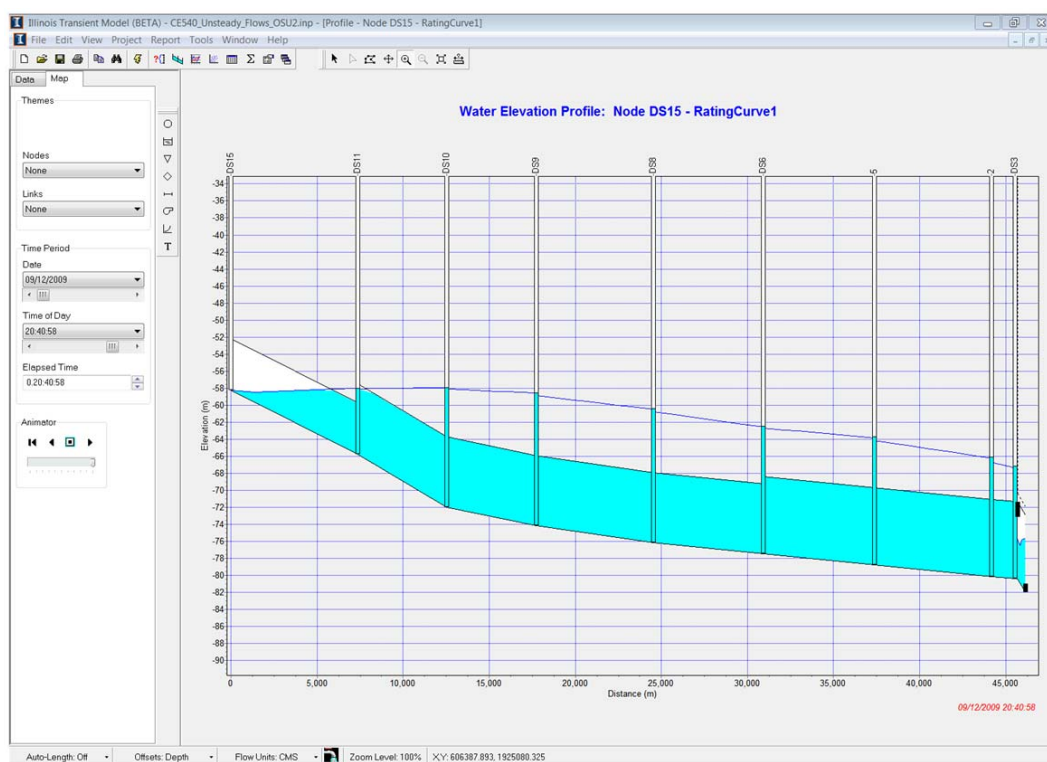


Figure 5.25: Hydraulic grade line snapshot between an upstream node and RatingCurve1 after 20 h 40 min 58 sec (Initial dry bed state, $a = 200 \text{ m/s}$).

Figure 5.26: Debug file intended for debugging of errors.

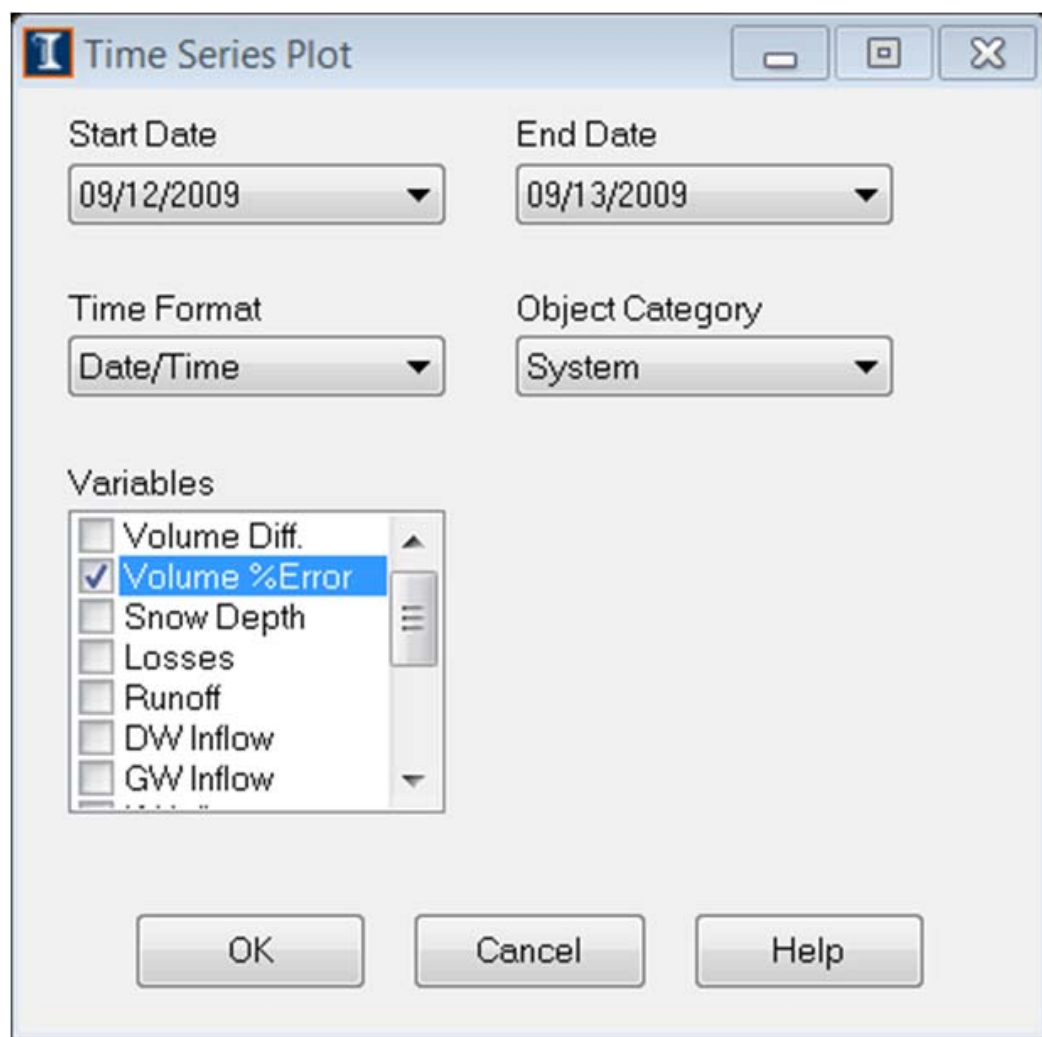


Figure 5.27: ITM interface for plotting time traces of volume errors.

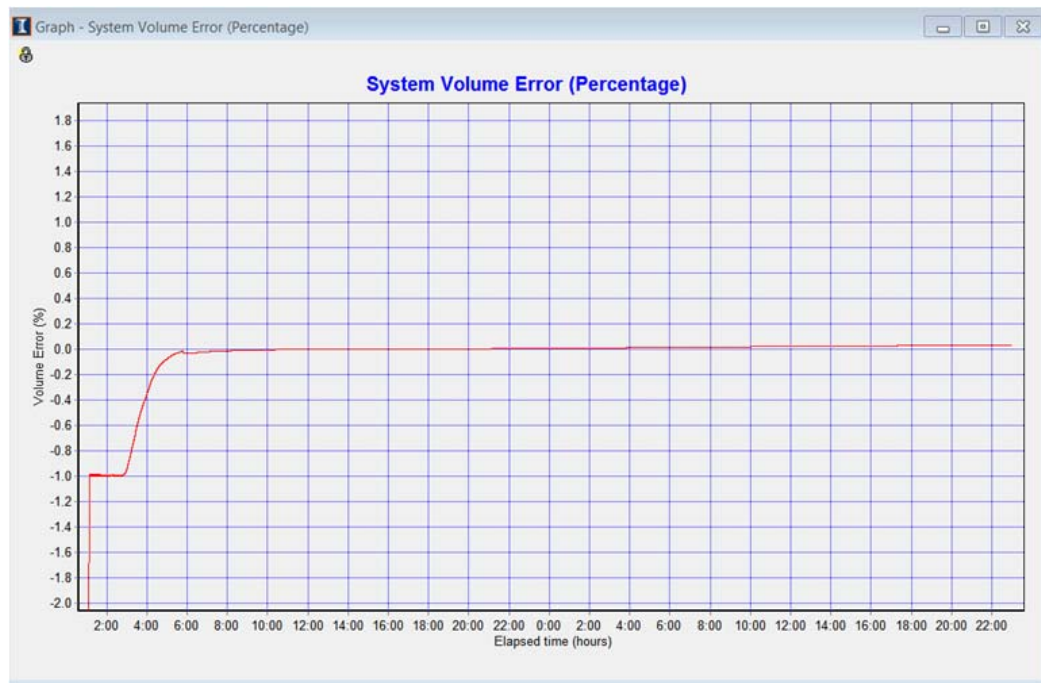


Figure 5.28: System volume error (%)[fine output time].

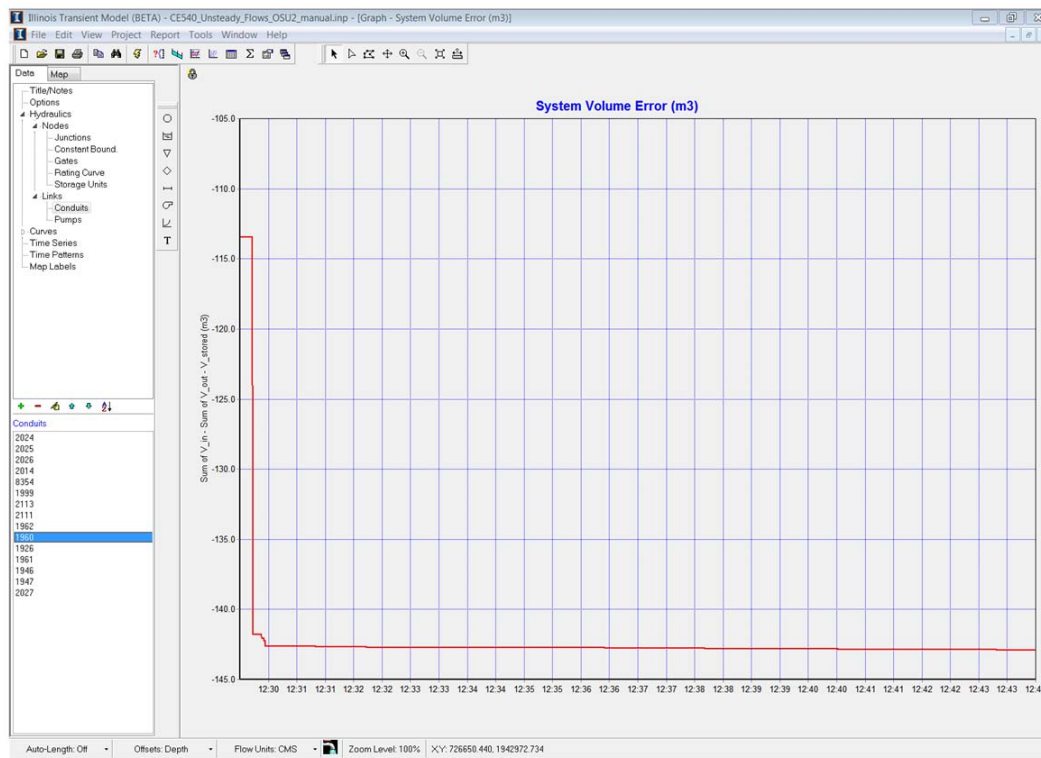


Figure 5.29: System volume error (m³)[fine output time].

References

- [1] Cardle, J. A. (1984). “An investigation of hydraulic transients in combination free surface and pressurized flows.” *Ph.D. thesis, Dept. of Civil and Mineral Eng., Univ. of Minnesota, USA.*
- [2] Cardle, J. A., Song, C. C. S. and Yuan, M. (1989). “Measurements of mixed transient flows.” *J. Hydraul. Eng.*, 115(2), 169-182.
- [3] Flow Science, Inc. (2005). “FLOW-3D v. 9.0 user’s manual”, Flow Science, Inc., Santa Fe, N.M.
- [4] Godunov, S. K. (1959). “Finite difference methods for the computation of discontinuous solutions of the equations of fluid mechanics.” *Math. Sbornik*, 47, 271-306.
- [5] Guinot, V. (2003). *Godunov-type schemes*, Elsevier Science B.V., Amsterdam, The Netherlands.
- [6] Hamam, M. A., McCorquodale, J. A. (1982). Transient conditions in the transition from gravity to surcharged sewer flow. *Canadian J. of Civ. Engng.*, 9, 189-196.
- [7] León, A. S. (2006). “Improved modeling of unsteady free Surface, pressurized and mixed flows in storm-sewer systems.” *Ph.D. thesis, Dept. of Civil and Environmental Engng., Univ. of Illinois at Urbana-Champaign, Urbana, IL.*
- [8] León, A. S., Ghidaoui, M. S., Schmidt, A. R., and García, M. H. (2005). “Importance of numerical efficiency for real time control of transient gravity flows in sewers.” *Proc., XXXI IAHR Congress*, Seoul, Korea.
- [9] León, A. S., Ghidaoui, M. S., Schmidt, A. R., and García, M. H. (2006a). “Godunov-type solutions for transient flows in sewers.” *J. Hydraul. Eng.*, 132(8), 800-813.
- [10] León, A. S., Ghidaoui, M. S., Schmidt, A. R., and García M. H. (2006b). “An efficient numerical scheme for modeling two-phase bubbly homogeneous air-water mixtures.” *Proc., ASCE-EWRI World Water and Environmental Congress*, Omaha, Nebraska.

- [11] León, A. S., Schmidt, A. R., Ghidaoui, M. S., and García, M. H. (2006c). “Review of sewer surcharging phenomena and models.” *Civil Engineering Studies, Hydraulic Engineering Series No. 78*, Univ. of Illinois, Urbana, IL.
- [12] León, A.S., Ghidaoui, M.S., Schmidt, A.R., García, M.H. (2007). *An efficient finite-volume scheme for modeling water hammer flows*. Contemporary Modeling of Urban Water Systems, Monograph 15, W. James (Editor in Chief).
- [13] León, A.S., Ghidaoui, M.S., Schmidt, A.R., García, M.H. (2008). An efficient second-order accurate shock capturing scheme for modeling one and two-phase waterhammer flows. *J. Hydraul. Engng.*, 134(7), 970-983.
- [14] León, A.S., Ghidaoui, M.S., Schmidt, A.R., García, M.H. (2009). Application of Godunov-type schemes to transient mixed flows. *J. Hydraul. Research*, 47(2), 147-156.
- [15] León, A.S., Ghidaoui, M.S., Schmidt, A.R., García, M.H. (2010a). A robust two-equation model for transient mixed flows. *J. Hydraul. Research*, 48(1), 44-56.
- [16] León, A.S., Liu X., Ghidaoui, M.S., Schmidt, A.R., García, M.H. (2010b). Junction and drop-shaft boundary conditions for modeling free surface, pressurized, and mixed free surface-pressurized transient flows. *J. Hydraul. Eng.*, 136(10), 705-715.
- [17] León, A.S., Gifford-Miears, C., and Choi, Y. (2013). Well-Balanced Scheme for Modeling Open-Channel and Surcharged Flows in Steep-Slope Closed Conduit Systems. *J. Hydraul. Eng.*, 139(4), 374-384.
- [18] LeVeque, R. J. (2002). *Finite volume methods for hyperbolic problems*, Cambridge Univ. Press, Cambridge.
- [19] OpenCFD, Ltd. (2007). “OpenFOAM User Guide”, OpenCFD, Ltd., Berkshire, United Kingdom.
- [20] Song, C. C. S., Cardle, J. A., and Leung, K. S. (1983). “Transient mixed-flow models for storm sewers.” *J. Hydraul. Eng.*, 109(11), 1487-1503.
- [21] Rossman, L. A. (2004). *Storm Water Management Model, Version 5, User's Manual*, U.S. EPA.
- [22] Toro, E. F. (2001). *Shock-capturing methods for free-surface shallow flows*, Wiley, LTD, Chichester, U.K.
- [23] Trajkovic, B., Ivetic, M., Calomino, F., and D'Ippolito, A. (1999). “Investigation of transition from free surface to pressurized flow in a circular pipe.” *Water Science and Technology*, 39(9), 105-112.

- [24] Vasconcelos, J. G., Wright, S. J., and Roe, P. L. (2006). “Improved simulation of flow regime transition in sewers: Two-component pressure approach.” *J. Hydraul. Eng.*, 132(6), 553-562.
- [25] Wylie, E.B., Streeter, V.L. (1983). *Fluid transients*. FEB Press, Ann Arbor, Michigan.
- [26] Yuan, M. (1984). “Pressurized surges.” *Master of Science thesis, Dept. of Civil and Mineral Eng., Univ. of Minnesota, USA*.